



Probabilistic Framework for Future Load Carrying Capacity Estimation of Corroded Metallic Railway Bridges under Heavy Axle Weight Trains

Ziliang Zhang¹; Geoff Watson²; David Milne³; William Powrie⁴; and Mohammad M. Kashani⁵

Abstract: Assessing the future load carrying capacity (characterized on UK railways by means of a route availability number) of historic railway infrastructure under heavy axle weight (HAW) train loads is important for operational and safety reasons. There are, however, considerable difficulties associated with the dual challenges of assessing current condition and potential future rates of degradation. In this paper, a probabilistic assessment framework for estimating the future route availability (RA) number of aging metallic railway bridges is proposed. The methodology is demonstrated with reference to a 37.7-m-long, single-track, three-span, half-through girder, early steel railway bridge. Nonlinear bridge responses to HAW train loads were evaluated using advanced finite-element models accounting for material plasticity, buckling, and potential unstable collapse. Possible failure mechanisms were explored using damage measures related to global and localized performance criteria. Aging of the metallic bridge was modeled assuming that time-dependent nonuniform corrosion dominates the deterioration process. Various model uncertainties, including those governing corrosion, were explicitly accounted for by sampling multiple realizations from a predefined multivariate statistical distribution. Future bridge capacity was quantified in the form of bridge deterioration equations (BDEs), i.e., bridge RA number as a function of age and train speed. Derived BDEs suggest that the bridge currently has sufficient capacity, despite nonuniform corrosion to a maximum depth of approximately 3 mm. However, if further deterioration occurs, HAW traffic accessibility could become compromised in three to four decades. The BDE formulation proposed in this paper provides a straightforward piece of information that can be used to support data-driven decision-making processes for both railway infrastructure owners and freight operators. DOI: 10.1061/JBENF2.BEENG-7409. This work is made available under the terms of the Creative Commons Attribution 4.0 International license, https://creativecommons.org/licenses/by/4.0/.

Author keywords: U-frame bridge; Freight trains; Buckling identification; Age-dependent fragility analysis; Latin hypercube sampling; UK railway.

Introduction

Background and Context

Reduced structural capacity of old metallic railway bridges due to ageing is a worldwide issue (Nakamura et al. 2019; Vagnoli et al. 2018). Such deteriorating infrastructure threatens the safe operation of heavy axle weight (HAW) traffic, which is of vital importance to

Note. This manuscript was submitted on November 1, 2024; approved on April 30, 2025; published online on August 19, 2025. Discussion period open until January 19, 2026; separate discussions must be submitted for individual papers. This paper is part of the *Journal of Bridge Engineering*, © ASCE, ISSN 1084-0702.

the economics of the rail freight sector (Martland 2013). Taking the UK railways as an example, the maximum axle load regularly permitted is currently 24.1 t. Higher axle loads up to 26.7 t, not uncommon for freight trains, are permitted only with specific dispensations, which the railway infrastructure owner has the right and obligation to withdraw without notice even if a minor reduction of capacity rating occurs on bridge infrastructures. This can potentially lead to major disruptions and economic losses for both the infrastructure owner and freight operators. Aside from immediate operational concerns, serious accidents involving HAW trains have also occurred as a direct result of heavily corroded bridge assets (RAIB 2010). Thus, there is a current need for a better understanding of the impact of HAW traffic on aging railway bridges to facilitate combined expertise- and data-driven decision-making processes on permitted axle loads and train speeds.

This study focuses on metallic bridges, which account for approximately 25% of all bridges recorded in a Network Rail's database of 24,951 bridges (Network Rail, unpublished data, 2023). Half of these metallic bridges are believed to be over 100 years old (Le and Andrews 2013). A recent review of the causes and consequences of metallic bridge collapses in the United Kingdom and the United States (Imam and Chryssanthopoulos 2012) found that corrosion was the principal cause of deterioration, with typical failure modes comprising severe buckling and shear on web plates. Deteriorated metallic bridges are particularly susceptible to HAW traffic because the high load magnitudes tend to reveal problems first. That is, the capacity of metallic bridges can be reduced significantly by corrosion, such that collapse may occur under the

¹Research Fellow, Dept. of Civil, Maritime and Environmental Engineering, Univ. of Southampton, Southampton SO17 1BJ, UK (corresponding author). ORCID: https://orcid.org/0000-0003-3821-8999. Email: ziliang.zhang@soton.ac.uk

²Senior Research Fellow, Dept. of Civil, Maritime and Environmental Engineering, Univ. of Southampton, Southampton SO17 1BJ, UK. ORCID: https://orcid.org/0000-0003-3074-5196. Email: g.watson@soton.ac.uk

³Senior Research Fellow, Dept. of Civil, Maritime and Environmental Engineering, Univ. of Southampton, Southampton SO17 1BJ, UK. ORCID: https://orcid.org/0000-0001-6702-3918. Email: d.milne@soton.ac.uk

⁴Professor, Dept. of Civil, Maritime and Environmental Engineering, Univ. of Southampton, Southampton SO17 1BJ, UK. ORCID: https://orcid.org/0000-0002-2271-0826. Email: w.powrie@soton.ac.uk

⁵Associate Professor, Dept. of Civil, Maritime and Environmental Engineering, Univ. of Southampton, Southampton SO17 1BJ, UK. ORCID: https://orcid.org/0000-0003-0008-0007. Email: mehdi.kashani@soton.ac.uk

passage of a single higher-than-usual load event (RAIB 2010). Factors such as fatigue (Imam and Righiniotis 2010) or fatigue corrosion (Macho et al. 2019) are not generally of primary concern for freight routes dominated by HAW traffic. Recent evidence has shown that local fatigue damage does not tend to influence the functionality of the whole bridge (Ahola et al. 2022; Kowal and Szala 2020) and that significant life remains between the initiation of a visually detectable crack and the failure of an element section (Fisher et al. 1990). Therefore, this study considered deterioration of metallic railway bridges subject to HAW loading as a predominantly time-dependent phenomenon (Imam and Chryssanthopoulos 2012), governed by corrosion-induced metallic plate wall thickness losses.

The state-of-the-practice in the assessment of metallic railway bridges does not generally incorporate degradation as a timedependent phenomenon. This is a natural consequence of the fact that, to date, railway bridge monitoring, maintenance, retrofitting, and replacement decisions have relied almost exclusively on expert evaluations of the most recently inspected and assessed bridge capacity, and engineering judgment of the current structural condition. Each bridge assessment is carried out at specified time intervals (visual inspections usually every 2 years and principal inspections every 5–6 years), independently of previous assessments. This means that a reassessment is carried out every time on principal inspection, potentially by different subcontractors employing their preferred analytical or numerical approaches as appropriate, and the bridge owner receives a final assessment report. Notwithstanding the merits of continuous inputs from expert site engineers who understand the bridges in detail, railway infrastructure owners often lack a tool to track the age-dependency of bridge structural capacity. There is also no framework under which consistent sets of numerical models can be meaningfully retained and improved over time for all weak bridges within a railway route or network. It is therefore not possible to assess bridge capacity in a structure-specific, condition-based manner or to estimate its future development.

Various bridge condition indices (BCIs) have been developed and implemented around the world (Akgul 2016; Darban et al. 2020; FHWA 2005; LoBEG 2010; MHURD 2003; Rummey and Dowling 2004). They assess overall bridge performance based on element-level conditions (Adams and Kang 2009), which can be tracked over time (DOT 2016). Most BCIs appear as a score ranging from 0 to 100, which is evaluated for each bridge, on the basis of element-level visual inspection and scoring according to a predefined hierarchy (Network Rail 2019), following bespoke algorithms. More significantly, various BCI-based predictive methods have also been proposed, which utilize historic bridge condition data to estimate future states. Deterministic approaches typically involve regression analyses on historic condition data (Bolukbasi et al. 2004; Morcous et al. 2002). Reliability-based approaches model degradation processes using methods such as lifetime analysis (DeStefano and Grivas 1998) or time-dependent survival analysis (Ng and Moses 1996). State-based probabilistic approaches typically use Markov chain-based bridge condition prediction models (Le and Andrews 2013) to describe the stochastic nature of bridge deterioration (Mauch and Madanat 2001), in which an initial state and a transition probability are typically defined and evaluated to estimate future states (Madanat et al. 1995). Attempts have also been made to correlate the evolution of condition states to estimates of residual structural capacity (Dizaj et al. 2021).

For three reasons, only limited use has been made of BCI-based predictive methods for tracking age-dependent performances of individual assets (M. Huband, personal communication, 2023a). First, the subdivision widths of element-level BCI scores are

usually too coarse to inform an age-dependent, structural-specific numerical analysis-the Bridge Condition Marking Index (BCMI) (Network Rail 2013), one particular BCI system used in the United Kingdom, provides an example, in that under extreme circumstances, a corroded web plate thickness can range from 10.3 to 2.7 mm without showing any difference in element-level BCMI score. Second, many BCI formulations do not necessarily correlate with true structural performance. Some marking systems could be designed in such a way that a structural element suffering from extreme localized corrosion can yield an element BCMI score better than another that is corroded more evenly but less severely. This is disputable considering the obvious possibilities of local geometric instability or strength-based total collapse owing to stress concentration. Third, field inspection procedures specified for most BCI are not intended to detect corrosion levels with high accuracy (M. Huband, personal communication, 2023b). BCI-based predictive methods are useful in that they can be easily applied to a large group of assets, hence are capable of forecasting the prospects for a transport infrastructure network at a macrolevel. However, they do not attempt to reflect accurate and detailed conditions of individual assets, for which rigorous consideration of structural details is needed.

Thus, there is a need for the development of a structural assessment framework that can estimate future structural capacities of railway bridges subjected to regular HAW traffic. Among other concerns, there are several technical challenges.

The first challenge is the high level of uncertainty associated with infrastructure deterioration, where the properties are variable both temporally and spatially. Apart from nonuniform corrosion of load-bearing elements of metallic bridges, uncertainties also manifest through the potential aging of bridge bearings and supports. The latter governs the boundary conditions of a bridge, hence its dynamic characteristics. The uncertainties are even greater when the intrinsically variable geometric and mechanical properties of the metallic materials on these bridges are considered. Materials such as cast iron, wrought iron, and early steel (in the United Kingdom, this refers to mild steel manufactured roughly since the 1890s, until its usages are gradually replaced by hightensile steel starting from the late 1930s) are all known to have different properties from modern steel, with potentially different statistical variabilities. These aspects complicate the problem and indicate the need for structural capacity to be evaluated using probabilistic tools.

The second challenge is the difficulty involved in making longterm estimates of corrosion of metallic materials typically found on old railway bridges. Acknowledging that corrosion is a complex phenomenon (Melchers 2003a), it is common to employ empirical or phenomenological corrosion models (Melchers 2003b) for practical use. These models typically deal with results from site-, structure-, and material-specific tests or structural monitoring campaigns by curve fitting (Abbas and Shafiee 2020; Melchers 1999; Paik et al. 2004; Rizzo et al. 2019; Soares and Garbatov 1999; Wang and Zhao 2016; Yang et al. 2019). Very few of them concern aging metallic railway bridges or their materials, especially those from around the 1900s (Moy et al. 2009). Furthermore, most corrosion models proposed to date do not consider a duration longer than 40 years (Decker et al. 2008). A way to improve the longerterm estimation capability of corrosion models was indicated in Melchers and Emslie (2016), where 4-, 8-, and 16-year equivalence of laboratory testing data was used in combination with fieldmeasured data from a 110-year-old bridge.

The third challenge concerns the determination of the spatial distribution of corrosion depths. To date, considerable efforts have only been made to numerically model the details of highly

localized corrosion nonuniformity (that is, individual corrosion pits) (Han et al. 2019; Paik et al. 2003; Silva et al. 2014; Sultana et al. 2015; Wang et al. 2018), and less attention has been paid to the characterization of corrosion nonuniformity on a macroscale (that is, at the typical dimensions of a structure or a structural member). Studies on realistic macroscopic distributions of corrosion depth have been mostly limited to marine engineering applications such as metallic ship girders (Saad-Eldeen et al. 2011) and ship decks (Garbatov and Guedes Soares 2008). For bridges, more attention has been paid to road/highway applications and far less to railways. Observations made on reinforced concrete decking, steel girder road bridges (Czarnecki and Nowak 2008; Gong and Frangopol 2020) suggest that corrosion generally concentrates on the top surface of bottom flanges along the beam direction, resulting from traffic spray salt build-up; corrosion is also likely to be distributed near the edges of girder web plates, especially toward the bridge bearings due to deck leakage.

Research Contributions and Novelty

The objectives of this paper are to establish a probabilistic assessment framework for estimating age-dependent structural capacity of metallic railway bridges and to demonstrate its feasibility and potential by means of a case study. Key contributions are as follows:

- Established probabilistic structural vulnerability assessment methodology is extended to be used predictively for evaluating future accessibility of aging metallic railway bridges for HAW traffic. Advanced analysis tools such as buckling and unstable collapse simulation and Latin hypercube sampling are incorporated.
- 2. A novel formulation referred to as bridge deterioration equation (BDE) is proposed, which estimates future allowable train axle weight as a function of age and permissible train speed. The route availability (RA) system used in UK railways is adopted in a case study, although it is also possible to incorporate other, alternative systems within the proposed framework.
- 3. Various model uncertainties, including those governing the long-term temporal evolution and macroscopic spatial distribution of corrosion depths, are featured within the framework. While data adopted from the literature or generated synthetically are used in the case study, research directions are highlighted toward which future field monitoring or laboratory testing campaigns could be targeted by railway infrastructure owners and researchers.
- 4. The use of two different load configurations for bridge assessment, referred to as equivalent load configuration (ELC) and axle load configuration (ALC), is compared to investigate how a single change of modeling assumption may affect assessment results.

Methodology

The proposed probabilistic assessment framework is an extension of the well-established concept of structural vulnerability assessment in the literature—initially developed for assessing structural performance against seismic hazard (Shinozuka et al. 2000) and subsequently adapted to evaluate the performance of a wide range of infrastructure against a variety of natural hazards, including scour (McKenna et al. 2021), flood (Khandel and Soliman 2021), hurricane (Ataei and Padgett 2013), tsunami (Petrone et al. 2017), and fire (Gernay et al. 2019). The focus of this paper is aging metallic railway bridges subjected to regular HAW

train traffic. The aim is to produce BDEs that are estimates of bridge capacity as a function of bridge age and permissible train speed. Fig. 1 presents a flowchart of the proposed assessment framework. Key steps are as follows:

1. Preliminary analyses:

- Conduct a desk study of the bridge and develop a nonlinear numerical model deterministically.
- · Identify the bridge modal properties.
- Identify train load configurations.
- Identify possible failure modes from the deterministic model and determine appropriate response thresholds with regard to specific damage measures.
- Verify and update the baseline model against structural monitoring data where possible.

2. Preprocessing:

- Identify the appropriate temporal evolution and spatial distribution of corrosion on the bridge.
- Identify model parameters to be treated as random variables (for generating multiple structure realizations) and those to be treated deterministically.
- Define *k* time snapshots at which subsequent analyses are to be conducted, covering the bridge age range of interest. For each of the *k* bridge ages, sample *n* bridge realizations of the random variables from the predefined multidimensional statistical distribution by means of Latin hypercube sampling (Jones et al. 2002; Olsson et al. 2003).
- 3. Batch finite-element analysis:
 - Carry out nonlinear static instability (Riks) analysis (SIMU-LIA 2014) for each of the $n \times k$ bridge models, in which predefined train load configurations are applied quasi-statically in a pushover manner—that is, from zero to a sufficiently large force magnitude.

4. Postprocessing:

- For each of the n×k analyses, identify the magnitude of structural demand at the instant of exceeding each damage measure threshold.
- Conduct structural vulnerability assessment to derive fragility functions (Zhang et al. 2023)—that is, the probability of exceeding a damage measure threshold as a function of structural demand.
- Estimate the BDEs using a user-specified confidence level and the proposed formulation.

Numerical Modeling

Structural Modeling

Overview of the Case-Study Aging Railway Bridge

A case-study bridge (Fig. 2) was selected to demonstrate the use of the proposed probabilistic framework for estimating the future capacity of aging metallic railway bridges. Constructed in 1903, it is a typical three-span, single-track, half-through girder, early steel bridge in the UK bridge inventory. The bridge sees regular HAW traffic because the railway it carries provides access to a stone quarry. Key structural dimensions and the position of the bridge relative to the railway line and the river, obtained from the original engineering drawings and the most recent Detailed Examination Report, are shown in Fig. 3. The central span of the bridge crosses the water, while the two side spans accommodate footpaths underneath the railway, along both riverbanks.

Structurally, the longitudinal load-bearing elements comprise two continuous main girders running along the sides of the bridge

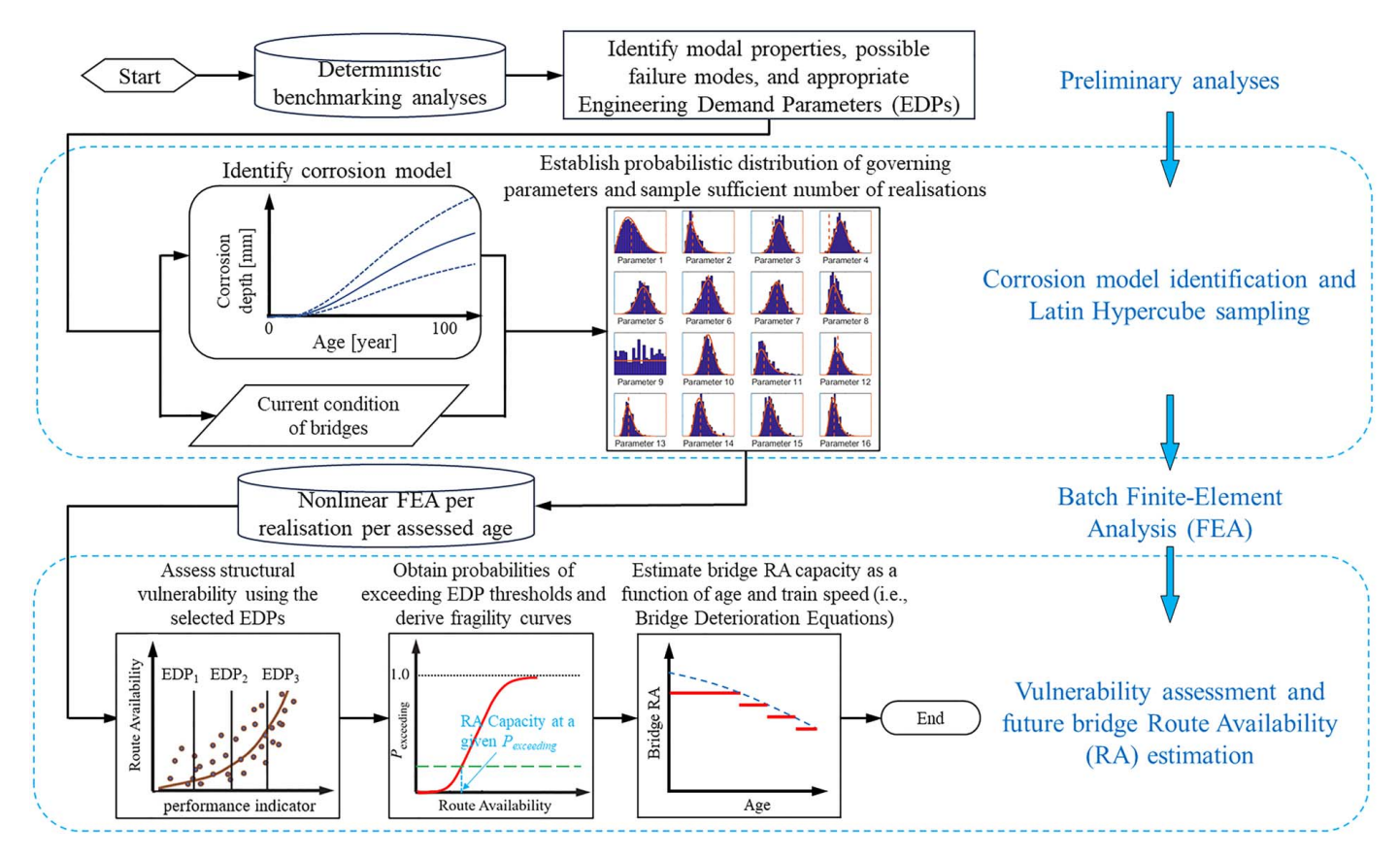


Fig. 1. Flowchart of the proposed probabilistic assessment framework for estimating the future capacity of aging metallic railway bridges.

and six discrete rail bearers, as shown in Fig. 3. The rail bearers are closed-ended I-beams, spanning between adjacent abutments/piers and supported at intervals by cross girders spanning between the main longitudinal girders. The three different arrangements of rail bearers within each bridge span are hereafter referred to as Rail bearers A, B, and C, as indicated in Fig. 3. Although the two main girders are structurally continuous, the parts over each bridge span with different lengths are referred to as Main girders A, B, and C for identification. The cross girders supporting the longitudinal rail bearers are themselves supported by the two main



Fig. 2. Upside elevation of the three-span, single-track, half-through type, early steel railway bridge examined as a case study.

girders and have identical geometry. In addition to the cross girders, adjacent longitudinal members are connected by transverse T-bars to enhance their stability. The metallic bridge deck as a whole is supported on masonry abutments and piers. Both piers are skewed at an angle of approximately 20°. Dimensions indicated in the original design drawing were adopted as the uncorroded condition, as there is no evidence suggesting any form of later structural modification or retrofit. Where the dimensions on the original drawing were unreadable, estimates were made based on similar members or according to their indicated sizes relative to other clearly labeled elements.

In the most recent Detailed Examination commissioned by the asset owner, noted defects were mainly corrosion-induced section losses near the edges of some structural members, accompanied by the fracturing of some nonstructural cover plates fitted between spans. These defects were not considered structurally critical (conclusion drawn by the inspectors). Nevertheless, the bridge was expected to deteriorate further, and the asset owner had expressed a concern that its capacity might be considered to be reduced in the next examination (P. Townsend, Personal communication, 2023).

Numerical Implementation

Numerical models of the case study bridge were developed using Abaqus (version 2023) (Dassault Systèmes 2023). A realization of the model is shown in Fig. 4(a). The metallic structural members of the bridge were modeled using the shell element S4R in Abaqus, while the flexibility of each bridge bearing was represented by equivalent bearing blocks, modeled using solid elements C3D8R in Abaqus [Fig. 4(b)].

Wall thicknesses of the metallic bridge members were modeled according to the design drawing, with corrosion (where present)

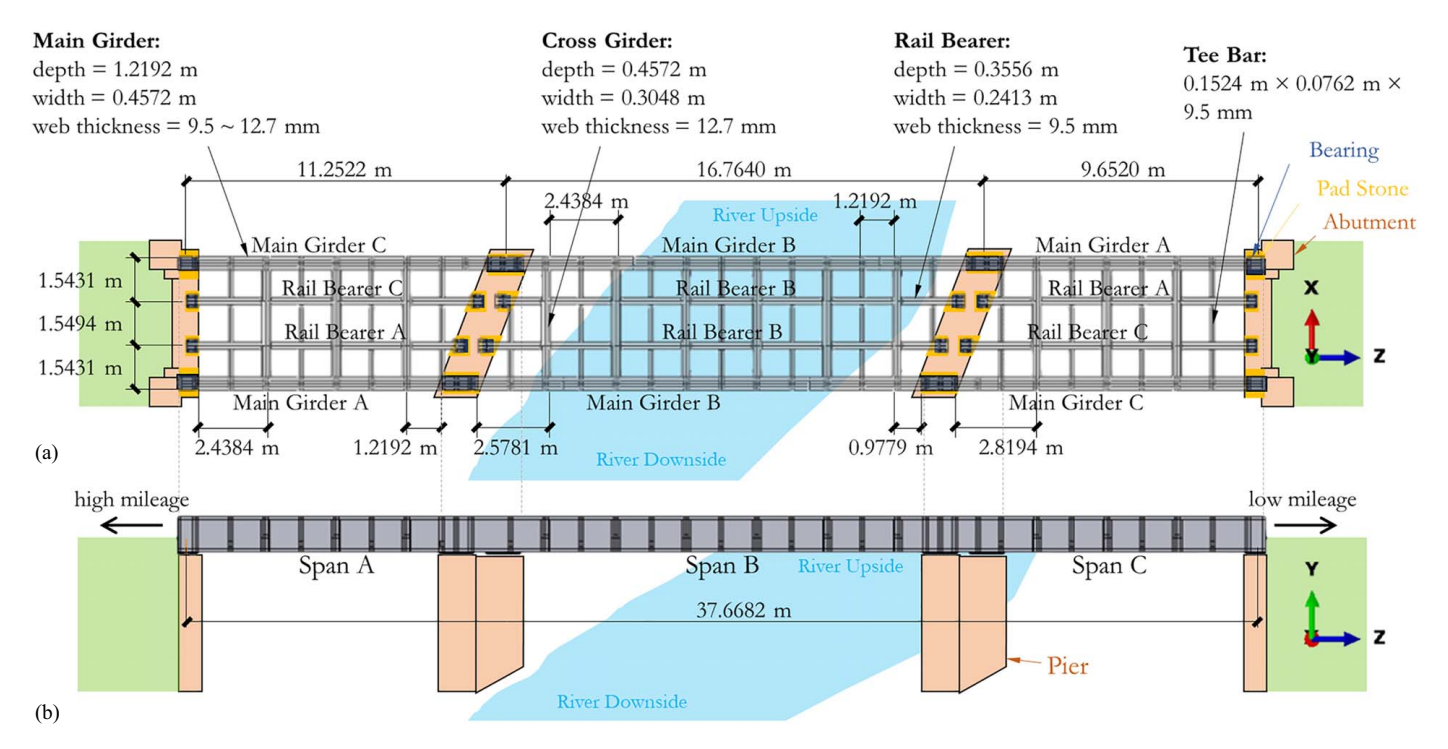


Fig. 3. (a) Plan; and (b) side view schematics of the case study railway bridge.

accounted for by applying nonuniform deductions to the original wall thicknesses. A total of 150 cross-sectional regions were defined in the model, accounting for variations in original wall thicknesses at different locations and to accommodate different corrosion zones. The early steel material of the bridge was considered to have an elastic modulus $E_{\rm steel} = 190.0$ GPa, yield strength $f_{y,\rm steel} = 239$ MPa, Poisson's ratio $v_{\rm steel} = 0.28$, density $\rho_{\rm steel} = 7.85$ t/m³, as suggested in Network Rail guideline NR/GN/CIV/025 (Network Rail 2006), and a nonlinear stress–strain response, as shown in Fig. 5 (Kossakowski 2021).

Each of the longitudinal structural members is supported in reality at the abutments and the piers by metallic bearing/bed plates on top of bedstones. The upper faces of the equivalent bearings were rigidly attached to the bottom surfaces of the main girders using tie constraints. The bottom faces of the equivalent bearings were fully fixed. The material of the equivalent bearings was modeled as linear-elastic with an elastic modulus $E_{\text{bearing}} = 6 \text{ MPa}$, Poisson's ratio $v_{\text{bearing}} = 0.495$, and density $\rho_{\text{bearing}} = 1.3 \text{ t/m}^3$. The equivalent bridge bearings were modeled with the same lateral dimensions as the original bearing plates, primarily to reduce fictitious local stress concentration on the lower flanges of longitudinal members. The thickness of the equivalent bearings was calibrated iteratively to be 0.06 m, to give lateral and vertical static initial stiffnesses of about 15×10^3 and 500×10^3 kN/m, respectively. These values match typical reported lateral (Han and Che 2021; Shuvalov et al. 2020; Zabel and Brehm 2009; Zhu et al. 2021) and vertical (Sipple and Sanayei 2015; Zabel and Brehm 2009) bridge bearing stiffnesses. The boundary conditions can have a significant impact on the calculated modal responses of the bridge, which are of importance because determining the dynamic increments for train loads requires the natural frequencies of each bridge span.

Nonstructural permanent loads on the bridge (ballast, sleepers, rails, and other equipment, including signaling cables) were accounted for as additional masses distributed evenly over the entire bridge deck area. The total self-weight of the bridge, as-built and

including these nonstructural masses, was determined to be approximately 120 t.

Train Load Modeling

Two different load configurations, both conceived based on relevant definitions in the Network Rail guideline NR/GN/CIV/025 (Network Rail 2006), were considered and compared using the proposed probabilistic framework. The first load configuration is referred to as the ELC, and the second is referred to as the ALC. Dynamic loads were included by the application of dynamic amplification factors to the static train loads, and transmission of train loads through the ballasted railway track was represented by the application of appropriate load dispersal rules specified in NR/GN/CIV/025 (Network Rail 2006).

RA System: A Brief Summary

The UK railway RA system (RSSB 2021) is used to determine which trains can safely travel on which sections of the UK rail network and at what maximum speed. Separate RA numbers are assigned for vehicles (demand) and bridges (capacity). A comparison of these two numbers then determines permissible bridges for a given vehicle.

The vehicle RA number is defined for a set of loads referred to as Type RA1 loading. It resembles an assumed, locomotive-hauled reference train comprising 12 sets of concentrated forces representing individual axles of the double-headed locomotives, followed by a trailing uniformly distributed load representing the wagons. The RA1 designation here refers to the load layout and is not the same as the vehicle route availability of RA1. Fig. 6 shows 20 British Standard Units (BSUs) of Type RA1 loading; this is by definition equivalent to vehicle route availability number RA10 without allowance for dynamic effects. Also, by definition, 10 BSUs of Type RA1 loading are equivalent to the vehicle route availability number RA0. Other vehicle RA numbers are correlated to the BSU quantity of Type RA1 loading -10 (e.g., 17 BSUs of Type

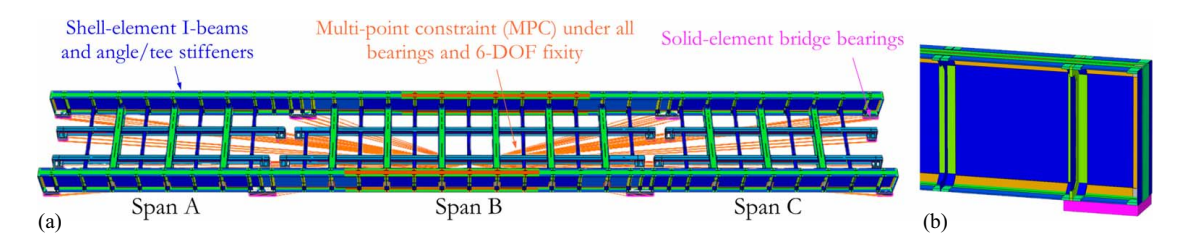


Fig. 4. (a) Overview of the finite-element model for the case study bridge; and (b) close-up view near one of the girder bearings, where differently colored/shaded regions on the shell elements indicate various as-built plate wall thicknesses. Note: The difference in color is used to indicate that the girder has various different plate thickness.

RA1 loading would correspond to a vehicle route availability RA7).

The calculation of bridge RA number is given in NR/GN/CIV/025 (Network Rail 2006) for various asset types. The essence of the method is to count the BSU quantity of Type RA1 loading that is within the structural capacity of all bridge elements (Gu et al. 2008). The capacity of a bridge depends on several factors; more or less complex methods can be used for this calculation, as required.

The RA system is known to be nonoptimal for defining/relating structural demand and capacity. While it gives separate RA designations to trains and bridges for ease of use, demand and capacity are somewhat coupled. For example, the bridge span in reality influences the level of structural demand imposed by a given vehicle and hence the route availability to it.

Load Configuration 1: ELC

Full calculation method for Network Rail specified equivalent train loads can be found in Network Rail (2006) and Clark (1997). To summarize, the process involves analytically solving the response envelopes of simply supported beams of various span lengths as they are traversed quasi-statically by 20 BSUs of Type RA1 loading. This calculation produces two values: (1) an equivalent uniformly distributed load (EUDL) corresponding to 20 BSUs of Type RA1 loading positioned for maximum bending; and (2) an end shear (ES) force corresponding to 20 BSUs of Type RA1 loading positioned for maximum shear.

The ELC adopted in this paper is essentially an extension to the equivalent distributed load approach given in NR/GN/CIV/025 (Network Rail 2006). In developing the ELC, train loading was modeled as a combination of EUDL and supplementary ES forces for simultaneous maximum bending and shear. First, the EUDL was applied to the six rail bearers of the case study bridge as it is. Concentrated forces were then added near either end of each rail bearer, without overlapping the bearings. These additional forces

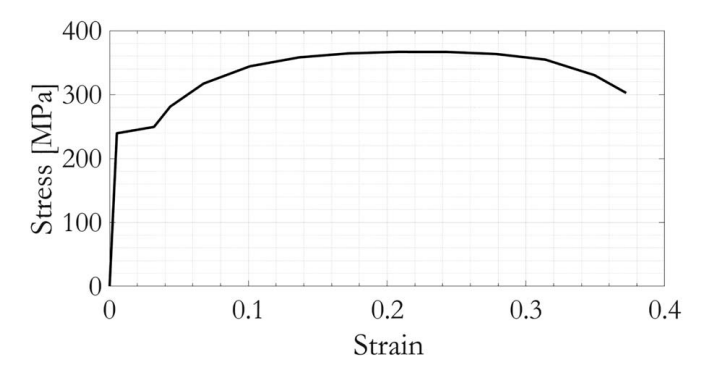


Fig. 5. Nominal stress–strain properties of early steel used for modeling the case study bridge. (Data from Kossakowski 2021.)

contributed negligibly to the bending moment on the bridge span, while increasing the maximum shear force to match the ES values listed in NR/GN/CIV/025. The known magnitudes of EUDL and supplementary ES forces are directly correlated to the BSU quantity of Type RA1 loading, hence also to vehicle RA numbers.

Load Configuration 2: ALC

The second load configuration adopted was the explicit application of a set of critically positioned Type RA1 loads. A series of deterministic static analyses was carried out to locate the critical position. Twenty BSUs of Type RA1 loading, as defined in Fig. 6, were moved quasi-statically along the bridge model in 1-m increments. All possible train positions were covered: starting from the instant when the first axle entered the first bridge span, all the way until the entire locomotive portion of Type RA1 loading had fully cleared the bridge so that the bridge was loaded solely by the 2×32.5 kN/m distributed force. The location of the Type RA1 loading most detrimental to the bridge was identified. This was adopted as the ALC in subsequent probabilistic analyses.

Dynamic Load Amplification

Dynamic effects were accounted for by multiplying the calculated static train loads by a dynamic amplification factor $(1+\varphi)$, where φ is the dynamic increment calculated from a set of empirically derived equations and is a function of train speed and bridge parameters. For train speeds up to 100 mi/h (160 km/h), dynamic increments for bending φ_{bending} and shear φ_{shear} are calculated as follows (Network Rail 2006):

$$\varphi_{\text{bending}} = \varphi_1 + \varphi_{11} \tag{1}$$

$$\varphi_{\text{shear}} = \frac{2}{3} \varphi_{\text{bending}} \tag{2}$$

where φ_1 = portion of dynamic increment accounting for the inertial response of the bridge; and φ_{11} = portion of dynamic increment accounting for wheel and track irregularities. These are calculated as follows:

$$\varphi_1 = \frac{k}{1 - k + k^4} \tag{3}$$

$$k = \frac{v}{4.47L_{\phi}n_0} \tag{4}$$

$$\varphi_{11} = \alpha \left[56e^{-(L_{\phi}/10)^2} + 50\left(\frac{\mathrm{Ln}_0}{80} - 1\right)e^{-(L_{\phi}/20)^2} \right] \text{ and } \varphi_{11} \ge 0$$
 (5)

$$\alpha = 0.0002v \text{ and } \alpha \le 0.01 \tag{6}$$

where v = permissible train speed (mi/h); $L_{\Phi} =$ determinant length of the member as defined in guideline NR/GN/CIV/025 (m)

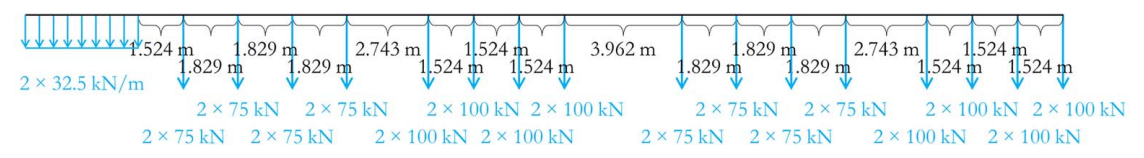


Fig. 6. Twenty BSUs of Type RA1 loading, as defined in NR/GN/CIV/025. The forces are herein denoted 2 × given magnitudes to reflect two rails per track. (Data from Network Rail 2006.)

(Network Rail 2006); n_0 = fundamental natural frequency of the structural member or bridge span (Hz); and L = span of the structural member from center to center of its supports (m). In the context of ALC, the more conservative (higher-valued) φ_{bending} was used in all cases because the applied forces already resemble an explicit train, rather than equivalent loads as in the case of ELC.

Load Transmission

The forces corresponding to RA0 to RA15 trains (i.e., 10–25 BSUs of ELC or ALC loads) calculated for the case study bridge were applied to the model following appropriate load dispersal rules given in Network Rail guideline NR/GN/CIV/025 (Network Rail 2006). With the rails supported on sleepers spaced at <800 mm intervals, 50% of the load was assumed to be transmitted to the sleeper directly beneath and 25% of the load to each of the two adjacent sleepers. Downward dispersal of stress from the sleepers through the ballast was taken to occur at 15° to the vertical. The dispersal area was further expanded concentrically, if necessary, to ensure that the pressure within the bridge decking at 200 mm above the upper surface of metallic structural members did not exceed 1 MPa.

These rules were used to calculate appropriate load transmission areas located along the lines of the two rails, together with equivalent patches of (possibly overlapping) pressure loads. This was done for both load configurations. The dispersed loads were then applied onto the intended areas via an idealized decking, representing the actual timber decking of the bridge. The decking in the numerical model is a near-weightless, linear-elastic, 15-mm-thick plate (not shown in Fig. 4), with elastic modulus $E_{\rm decking}$ = 190.0 GPa. This idealized decking plate was tied to the upper flanges of rail bearers and cross girders. The transverse T-bars were not connected to the decking because they are intended and designed only to provide out-of-plane stability to the longitudinal structural members.

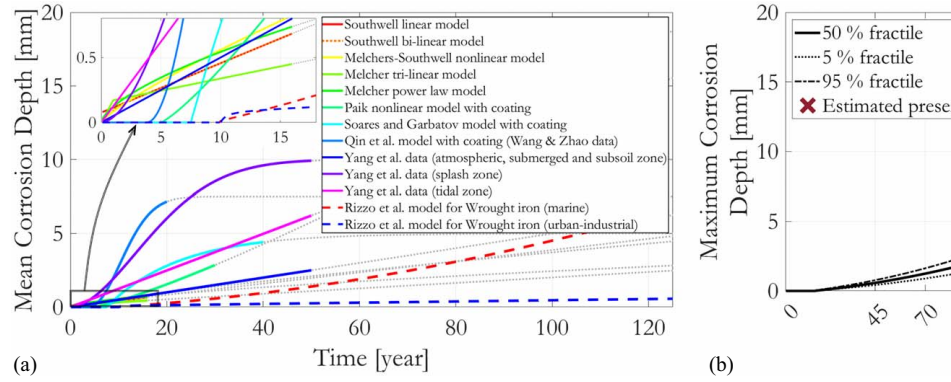
Bridge Corrosion Modeling

Temporal Evolution of Corrosion Depth

It is possible to incorporate multiple corrosion models to multiple corrosion zones (Khodabux et al. 2020; Melchers and Emslie 2016) on a bridge, as appropriate; a selection is shown in Fig. 7(a). In the absence of information specific to the case study bridge, a single corrosion model [Fig. 7(b)] was adopted here for all corrosion zones. The shape of the corrosion curve was adapted from Rizzo et al. (2019), while the corrosion rate was adjusted so that the mean value of nominal corrosion depth d_n (summed on both sides of metal plates) calculated for the current age corresponded broadly to the field observations reported in the most recent Detailed Examination Report. The exponential corrosion model outlined in Rizzo et al. (2019) is provided for early ferrous metal and is said to be applicable for 125 years. This exponential corrosion growth law was extended herein, on the basis of the calibration at the current bridge age of approximately 120 years. In practice, estimations made for a much shorter future period (e.g., 5-10 years from the present time) are vital for bridge owners and freight operators from an operational point of view to plan for potential future rerouting. The estimations also need to be regularly updated by recalibrating the model using the latest observed corrosion conditions. Longer-term estimations (e.g., beyond the typical applicable estimation period of around 40 years for most other corrosion models) can thus be taken more qualitatively rather than quantitatively. Given these considerations, the applicable estimation time given in Rizzo et al. (2019) is used in this work for completeness of the demonstration.

Spatial Distribution of Corrosion Depth

Deterioration in each corrosion zone may be assumed uniform (Czarnecki and Nowak 2008; Melchers 2018; Melchers and Emslie 2016) for design and assessment purposes (Bai et al. 2015). This is because uniform corrosion is of interest for degradation of overall



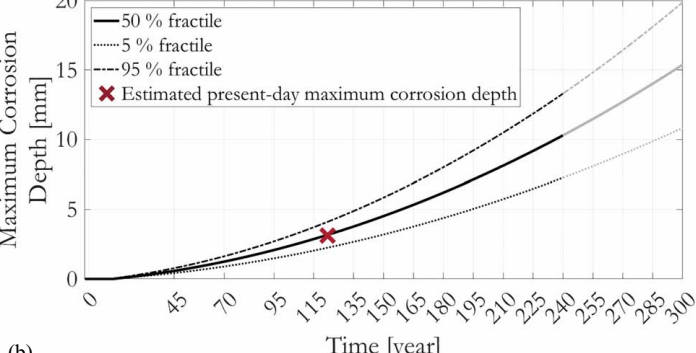


Fig. 7. (a) Various corrosion models in the literature expressing corrosion depth as a function of age (Abbas and Shafiee 2020; Melchers 1999; Paik et al. 2004; Rizzo et al. 2019; Soares and Garbatov 1999; Wang and Zhao 2016; Yang et al. 2019); and (b) the corrosion model adopted in this study, calibrated based on the shape of the corrosion curve recommended by Rizzo et al. (2019).

structural strength, including plates and structural members, while nonuniform or pitting corrosion has been found more important for containment applications such as pressure vessels (Melchers 2003b). If needed, some form of corrosion distribution can be superimposed onto the general corrosion depth d_n to reflect nonuniformity (Tamakoshi et al. 2006).

In this study, macroscopic spatial nonuniformity of corrosion was categorized into four zones: (1) the main girder web, (2) the main girder upper flange, (3) the main girder lower flange, and (4) secondary members. For the primary load-bearing elements (i.e., the main girders), corrosion distributions were defined inplane for each of the three surfaces of the I-section main girders. For secondary load-bearing elements (cross girders and rail bearers) and other elements (T-bars), corrosion nonuniformity was considered in a general sense by attributing the entire deck area to only one corrosion zone in the x-z plane (using the coordinate system defined in Fig. 3). Potential in-plane variations of corrosion depth on individual metallic plates were thus neglected. This resulted in a total of 7 corrosion zones and 55 nonuniformly corroded wall thickness definitions in Abaqus. For each of the k bridge ages (time snapshots) assessed, synthetic macroscopic spatial distributions of corrosion depth were sampled for each of the seven corrosion zones to produce $(7 \times n)$ corrosion distribution realizations. The generated spatial distribution factors, as a two-dimensional matrix representing a surface, took the shape of the probability distribution functions (PDF) of two-dimensional beta distributions. The full range of beta distribution function parameters was selected so that randomly sampled distributions would have a high probability of resembling qualitatively the observed trends of corrosion reported in Czarnecki and Nowak (2008), Gong and Frangopol (2020), and RAIB (2010). That is, heavier corrosion is more likely to occur toward the edges and joints of metallic plates on main girders and toward the edges of the bridge decking area for the secondary elements.

Fig. 8 summarizes the steps followed to generate synthetic spatial distributions of corrosion in this study. Within each corrosion zone, the overall degree of corrosion was governed by the nominal corrosion depth d_n . d_n was then multiplied by a corrosion distribution factor, $0 < f(x, y) \le 1$, to produce a discrete two-dimensional

field of nonuniform corrosion depth. f(x, y) is a function of location coordinates, e.g., x and y, mapping the planar area covered by a corrosion zone. Variability of corrosion depth comprised two portions: global $f_{\text{global}}(x, y)$ and local $f_{\text{local}}(x, y)$. $f_{\text{global}}(x, y)$ was defined by the PDF of a two-dimensional joint beta distribution, while $f_{\text{local}}(x, y)$ was defined by a two-dimensional sinusoidal function:

$$f_{\text{local}}(x, y) = 0.05 \sin\left(\frac{2\pi x}{\lambda}\right) \cos\left(\frac{2\pi y}{\lambda}\right) + 0.95$$
 (7)

f(x, y) can be computed as follows:

$$f(x, y) = \frac{f_{\text{global}}(x, y) \odot f_{\text{local}}(x, y)}{\max[f_{\text{global}}(x, y) \cdot f_{\text{local}}(x, y)]}$$
(8)

where \odot = element-wise multiplication operator; λ = 0.4 is a characteristic wavelength governing the dimensions of local wall thickness variability; and max[] = maximum function that finds the maximum element within a matrix.

Each of the 55 nonuniformly corroded wall thickness definitions was implemented in Abaqus using a mapped analytical field. Discrete field values were imported and applied to different sections defined in the model by mapping the specified x-, y-, and z-coordinates to the corresponding locations. A minimum wall thickness of 1 mm was considered to avoid numerical issues.

Deterministic Responses of the Case Study Railway Bridge

This section considers the calculated responses of the bridge in deterministic analyses. Modal responses are first presented to provide insights into the bridge dynamic characteristics. This is then supplemented by a nonlinear dynamic time history analysis of the bridge at its current age. Typical quasi-static nonlinear bridge responses are then outlined in relation to the definition of four structural performance criteria. This is followed by an exploration of the effect of age-dependent corrosion on bridge responses and the determination of the critical position of explicit Type RA1 loading on the bridge.

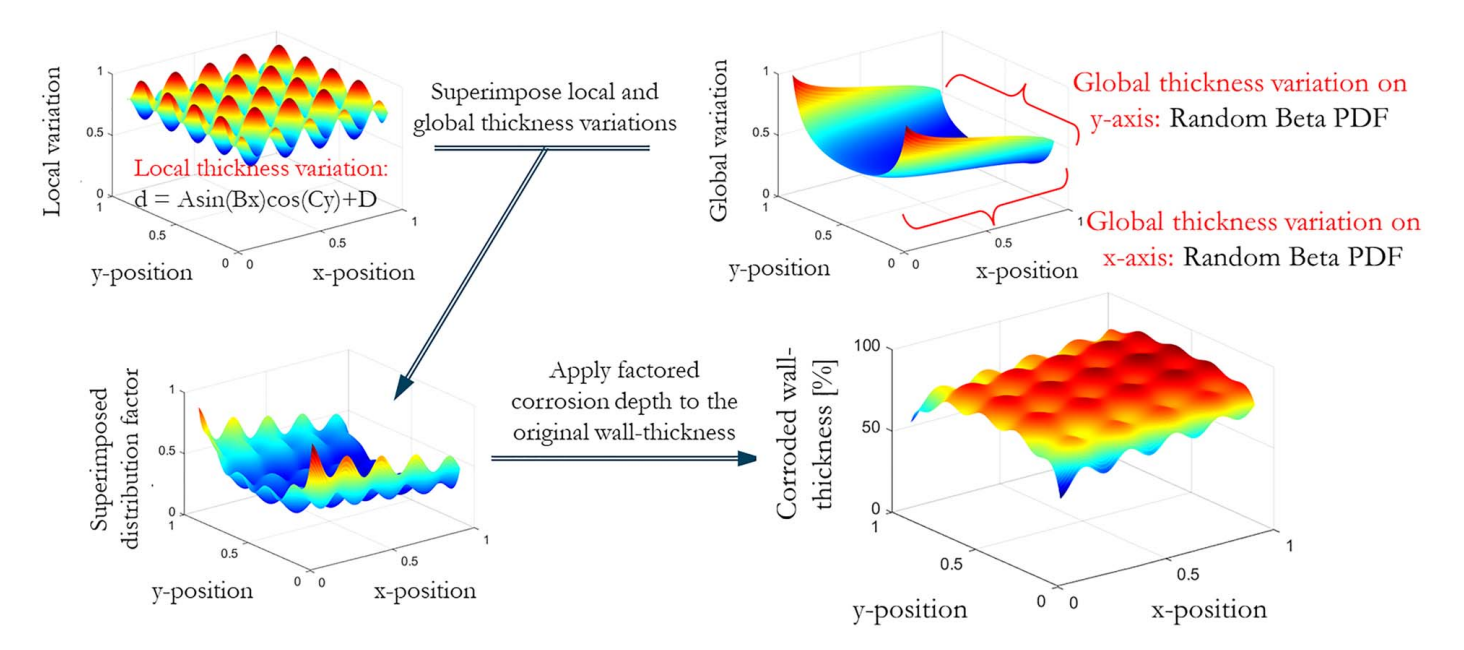


Fig. 8. Flowchart for generating a synthetic nonuniform spatial distribution of corrosion depths.

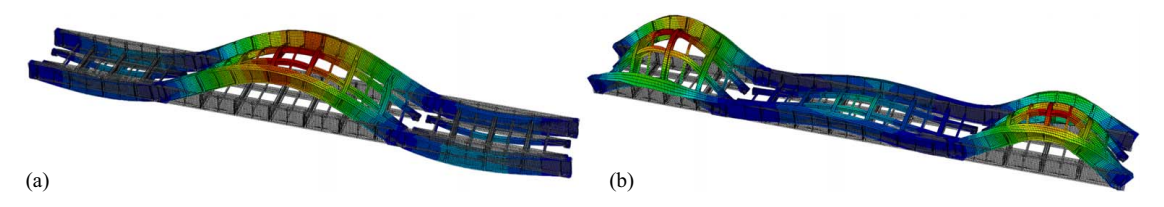


Fig. 9. Mode shapes of (a) first; and (b) second vertical natural modes involving, respectively, the center span at 6.4 Hz and the two symmetrical side spans at 11.2 Hz.

Modal Responses

Fig. 9 shows the numerically simulated shapes of the first and second vertical vibration modes of the bridge as built. Any contribution to the stiffness from the bridge decking was neglected. The natural frequencies are 6.4 and 11.2 Hz, respectively. The vertical dimensions, elastic modulus, and Poisson's ratio of the equivalent bridge bearings could all influence the calculated natural frequencies. Further, the first vertical mode at 6.4 Hz was found to be almost exclusively associated with the vibration of the center span, and the second vertical mode at 11.2 Hz was found to be almost exclusively associated with the two side spans. There was no combined vertical mode of vibration, probably because the three bridge spans are joined structurally only by the two continuous main girders. These calculated natural frequency values were used to determine the dynamic increment φ for each span. The natural frequencies of vertical vibration of each bridge span were found to reduce by approximately 15% at a bridge age of 240 years, owing to corrosion.

Dynamic Responses Subjected to Linear-Elastic Load

A nonlinear dynamic time history analysis of the bridge was carried out to further understand its dynamic characteristics. The load case

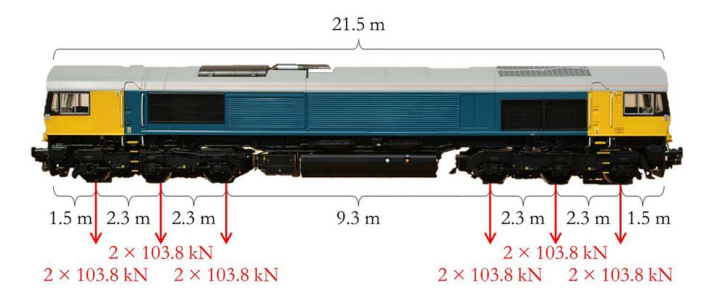


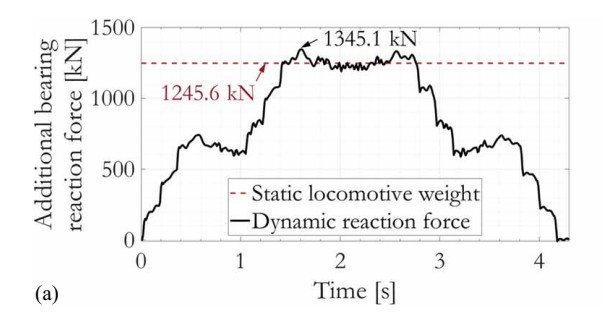
Fig. 10. Approximated dimensions and axle loads of the Class 66 locomotive. (Image by authors.)

was a single Class 66 locomotive (Wikipedia 2024) traversing the bridge at a constant speed of 30 mi/h (13.4 m/s). Locomotives of this class cross the bridge regularly and have an axle load rating of RA7, to which the bridge response is known to be linear elastic (and confirmed so by the numerical analysis).

The approximate dimensions and axle loads of a Class 66 locomotive are shown in Fig. 10. The axle loads, dispersed as appropriate, were applied as moving loads on the bridge decking along each of the two rails. The idealized decking plate in the model was extended beyond each end of the bridge to accommodate the entire locomotive if it had not yet entered or cleared the bridge. A 1.6% Rayleigh damping ratio was applied based on the two numerically determined vertical vibration modes.

The time history of the total bridge reaction force, after subtracting the bridge static self-weight, is shown in Fig. 11(a). The instants at which each of the two train bogies enters and leaves the bridge are clear. The dynamic nature of the applied load resulted in a maximum reaction force amplification of approximately 8.0%. This compares satisfactorily with the inertial response element of the empirically calculated dynamic increment for shear on Span B for trains traveling at 30 mi/h: $\varphi_{1,\text{shear}} = 2/3 \times \varphi_{1,\text{bending}} \approx 7.3\%$. Wheel and track irregularities were not accounted for in this exercise because these effects were expected to be negligible. This was confirmed by the calculated track irregularity portion of the dynamic increment, φ_{11} , of zero.

The time history of vertical deflection at the center of Span B is shown in Fig. 11(b). Span B had an initial static deflection of 2.7 mm and a maximum dynamic deflection of 8.5 mm. The instants when the two train bogies were positioned at the center of Span B, causing maximum deflection, are at around 1.5 and 2.6 s. Dynamic amplification for deflection was approximately 3.7%. Furthermore, it was found that the degree of corrosion had practically no effect on bridge deflection. This is consistent with engineering judgment, considering that the second moment of area of the I-beam cross sections is dominated by its depth, which changes negligibly due to corrosion.



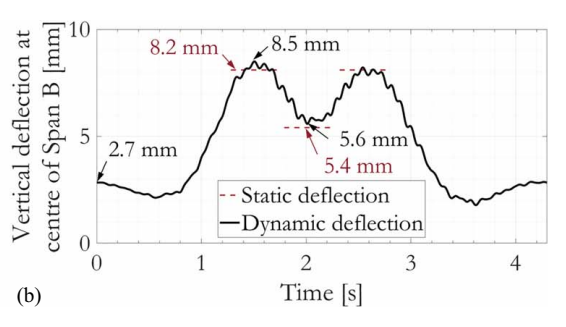


Fig. 11. Linear-elastic dynamic time history responses of the bridge subjected to a single Class 66 locomotive traveling at 30 mi/h (13.4 m/s): (a) total additional reaction force on bridge bearings; and (b) magnitude of vertical downward deflection at the center of Span B.

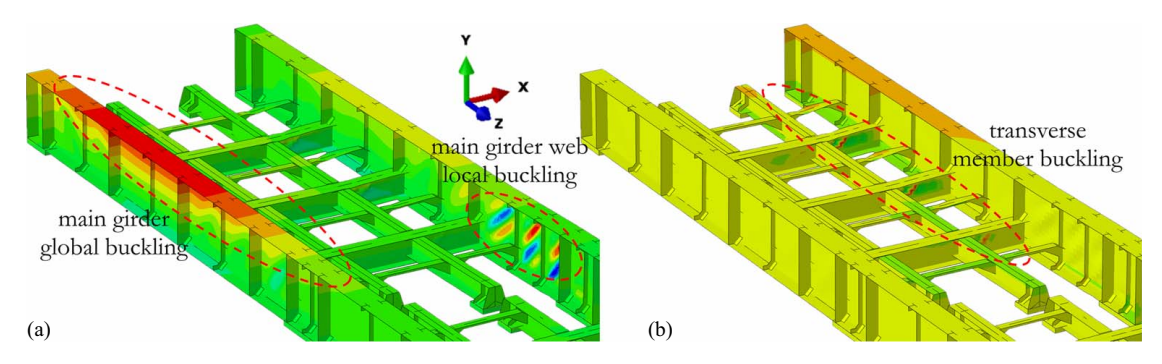


Fig. 12. Contour plot of (a) *x*-axis displacement; and (b) *z*-axis displacement of an extreme case scenario, where three possible buckling classes are simultaneously visible.

Quasi-Static Nonlinear Responses in Relation to Structural Performance Criteria

Four potential structural failure mechanisms were identified for the case study bridge: global buckling of main girders, local buckling on main girder plates, buckling of transverse members, and material yielding. Fig. 12 illustrates an extreme case scenario in which all four mechanisms occurred simultaneously; three classes of buckling are visible in terms of excessive out-of-plane deformations.

Quantitative identification of buckling can be challenging. Finite-element analyses of a complex structural model usually led to a variety of local, global, or distortional buckling shapes at various locations, most of which appear to be coupled (Ádány et al. 2010; Nedelcu and Cucu 2014). Identification is typically based on visual inspection, which is time-consuming and subjective (Ádány et al. 2010). In this study, a combined numerical and judgment-based approach was adopted. For global and local buckling of the main girders, representative response variables were first selected as damage measures with appropriate threshold values. These thresholds correlated with the onset of global or localized buckling and were determined on the basis of engineering judgment supported by a large number of observations. The quantified damage measures were then used to develop an automated identification process, implemented in Matlab (version 2023a) (Math-Works 2023). Identification of transverse member buckling was done primarily via visual inspection, which was assisted by finding highly nonlinear force-displacement responses at probable locations using a Matlab script to narrow down suspected cases and provide qualitative confirmation to the identified cases. The methods of buckling identification used herein are not universal and may not be suitable for bridges of different structural forms. However, changes in potential failure modes or criteria do not affect the validity of the proposed assessment framework.

Global Geometrical Nonlinearity: Main Girders

I-beam global instability can lead to excessive out-of-plane deformation of the main girders and is resisted in half-through type bridges by the structural behavior known as U-frame action (Canning and Kashani 2016). The rigidity provided by the U-frame depends on cross girders, web stiffeners, and the connections between the two (SteelConstruction.info 2024), which stabilize the top flanges of the main girders (BSI 2000). Fig. 13 shows the typical force—displacement response at the center of the top of a main girder, with the overall bridge response governed by the global buckling mode. The force refers to the total applied train load, and the displacement is the out-of-plane deformation monitored at the center of the top of the main girder within a bridge span. The slope of the response curve gradually decreases as the deflection increases.

In theory, the magnitude of the applied load will reach a maximum, at which point the slope of the response curve reduces to zero. This critical point can be considered as the onset of unstable collapse. Any reserve of strength between the initiation of girder global buckling and unstable collapse is likely to be insignificant (Ádány et al. 2010). The onset of global buckling in the main girders was thus quantified at the point at which the slope, K, of the force versus out-of-plane displacement relation reduces to a given fraction of its initial value, $K_{\rm init}$, and does not recover in subsequent load increments:

$$K < 0.1K_{\text{init}} \tag{9}$$

Local Geometrical Nonlinearity: Main Girders Plates

If the response of the main girder is dominated by localized plate buckling, the force versus out-of-plane displacement response of the top flange of the locally buckled girder segment will exhibit nonlinearity, as also shown in Fig. 13. Regardless of the precise location of locally concentrated plate deformation, its development alleviates the global out-of-plane deflection around that area. The latter would not increase in proportion to the total applied load and may even reduce if the applied load increases further. The post-buckling reserve of strength before a strength-based single-point failure occurs is, in this case, considerable.

The onset of local plate buckling of the main girders was thus identified at the point at which K increases above a given proportion of K_{init} :

$$K > 1.5K_{\text{init}} \tag{10}$$

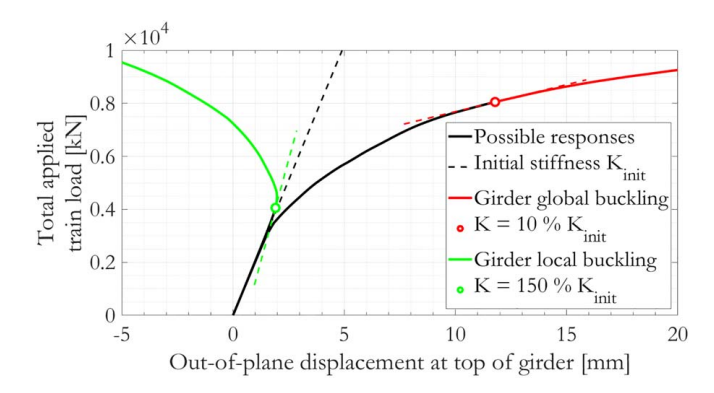


Fig. 13. Identification of global and localized instabilities of the main girders based on force versus out-of-plane displacement response curves.

Buckling of Transverse Members

In the studied bridge, transverse and longitudinal members form a stiff lateral grillage. Thus, in simulations, transverse member buckling never occurred as a standalone failure mechanism. When it did occur, it was always coupled with either local or global buckling of main girders and often quickly after the onset of material nonlinearity. This might be attributed to the depth of the transverse members being much shallower than that of the main girders. The coupled buckling mechanism might trigger simultaneous failure on multiple transverse members within a single bridge span, leading to the overall instability of the U-frame bridge cross section.

Based on these observations, identification of transverse member buckling was primarily by visual inspection [an example is given in Fig. 14(a)] of the simulation results and engineering judgment. Analysis cases where high values of von Mises stress (>95% of the yield value) occurred on transverse members were flagged for inspection. The onset of buckling was then manually identified considering (1) visual confirmation of wavelike or distorted deformed shapes indicative of local or distortional buckling and (2) numerical confirmation of a highly nonlinear force—displacement response at or adjacent to the suspected buckled area [as shown in Fig. 14(b)].

Material Nonlinearity

Material yielding in simulations was monitored at all locations across the bridge with two exceptions. The first was on shell elements that were directly tied to the elastic equivalent bearing blocks, as responses there can be fictitious. The second was the localized yielding at the bottom of each stiffener. This is because if the localized yielding does not develop further within the depth of the stiffener, it will not result in failure. The onset of material yielding can be detected when the equivalent plastic stress (PEEQ) becomes greater than zero. To rule out fictitious yielding responses at a single finite-element node (due, e.g., to a small area of distorted finite-element mesh), a small amount of plastic strain was allowed:

$$PEEQ > 0.01\%$$
 (11)

If an analysis case aborted numerically before reaching the prescribed load and no buckling was detected, that case was counted as a failure due to material yielding.

Effect of Corrosion on Bridge Responses

Fig. 15 compares typical x-axis displacement responses on Span A of the bridge at different ages. The comparison was made between simulations, each assigned the nominal maximum corrosion depth d_n at each age. Random spatial distribution of corrosion depths was

introduced at each examined bridge age; an example is shown in Fig. 16. All cases were subjected to the same ELC train load, equivalent to 25 BSUs of Type RA1 loading (RA15), without dynamic amplification.

Up to an age of 115 years, no sign of local buckling was observed. Globally, inward deformation of the main girders was most apparent on the top flange as a result of U-frame action, the amplitude of which increased monotonically with bridge age. Main girder A generally suffered greater global deformation than Main girder C, likely due to the skewness of the bridge piers.

The development of corrosion at and beyond an age of 135 years resulted in various degrees of local buckling, identified primarily on the web plates of the main girders. Buckled web plates were often located near the end supports of the bridge span, where shear forces on longitudinal members were greatest. The web plate most susceptible to buckling was that at the continuous end of Main girder A, located toward the bridge pier. This may also be attributed to the shorter length of Main girder A compared with C. Nonetheless, the onset of local web buckling did not always occur at the same location owing to the random spatial distribution of corrosion. Web plates on the rail bearers and cross girders were found to be comparably stressed to those on the main girders but generally did not exhibit stability issues. This was probably a result of their shallower cross-sectional depth and mutual support.

Beyond a bridge age of 180 years, simultaneous local buckling on multiple web plates and higher local buckling modes became possible owing to severe general corrosion throughout the entire web area of the girders. The development of local buckling in web plates tended to alleviate global out-of-plane responses at the top flanges of the main girders. As examples, the x-axis displacement response at the top flange of Main girder A in Fig. 15 reduces from 115 years to 180 years, and the out-of-plane displacement at the top of Main girder C at an age of 195 years was the smallest. This mechanism effectively inhibited the onset of main girder global buckling and the subsequent local buckling of the main girder top flanges in most cases. This behavior is generally desirable because locally buckled thin-walled members often have significant postbuckling reserve, whereas global buckling typically renders the member with little postbuckling strength and is thus likely to have more catastrophic consequences.

Critical Position for ALC (Load Configuration 2)

Twenty BSUs of Type RA1 loading, as defined in Fig. 6, were moved quasi-statically along the bridge model to determine the critical load position. The critical Type RA1 loading was referred to as the ALC and was used in subsequent probabilistic assessments. For simplicity, the ALC was identified deterministically using the uncorroded bridge model.

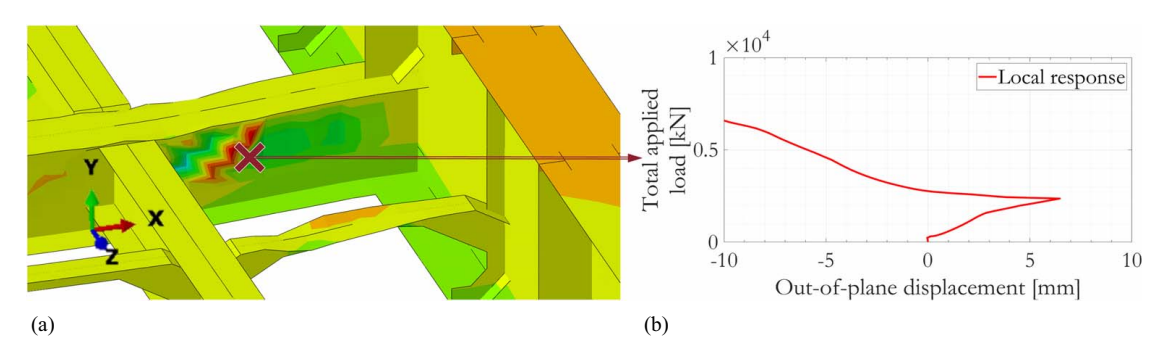


Fig. 14. Identification of transverse member buckling: (a) contour plot of out-of-plane (*z*-axis) displacement; and (b) total applied load versus out-of-plane displacement monitored adjacent to the buckled location.

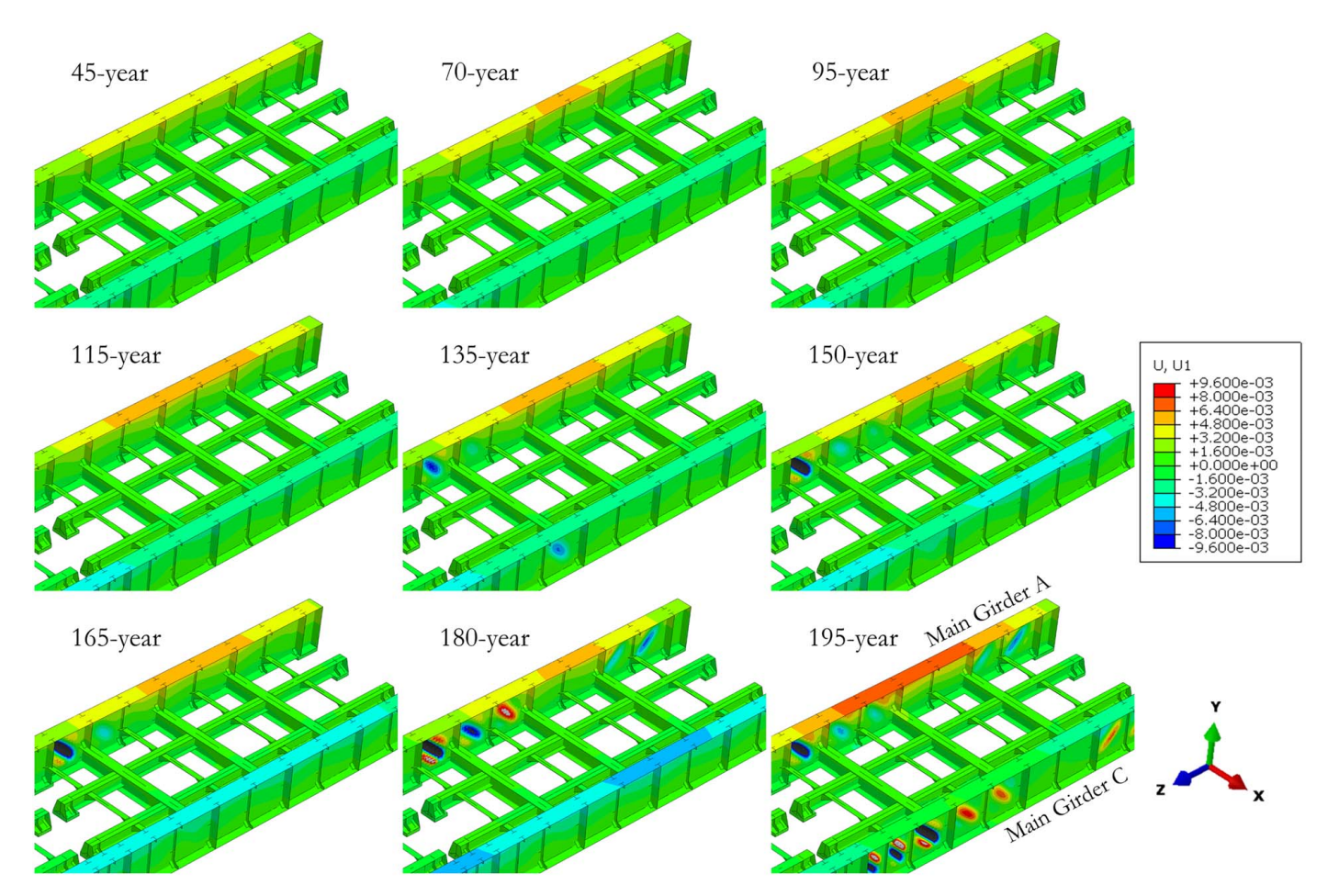


Fig. 15. Effect of aging on the *x*-axis displacement response on Span A, given RA15 train load in the ELC. The color spectrum corresponds to *x*-axis displacements ranging from −9.6 to 9.6 mm. Note: Color is used to highlight the buckling pattern and their relative severity with respect to age.

The uncorroded bridge remained linear-elastic when subjected to 20 BSUs of Type RA1 loading, and no global or local instabilities occurred. Stress- and displacement-based responses were examined, as summarized in Table 1, which gives the overall maximum deflection values together with the associated load position. Here, the load position is defined as the distance between the high-mileage end of the bridge and the leading axle of the ALC train, moving toward the low-mileage direction.

Critical structural demands on each span were often imposed by the heavier and more densely located axles (that is, the four 2 × 100 kN point loads). While the two side spans were geometrically symmetrical, Span A always sustained more critical structural demands. Visualization of the critical Type RA1 loading positions indicated that when Span A was critically loaded, Span C was often unloaded as the moving train had not yet physically reached it.

However, when Span C was critically loaded, Span A was always also loaded by either the trailing locomotive or the wagons. This asymmetry, owing to the directionality of the traveling train, affected bridge responses. It was evident that the overall critical loading scenario for the bridge was not when all its spans were fully loaded (thus sustaining the highest total external load), but when the partly continuous bridge was loaded on only the first or the first two spans, with no force acting on the remainder to in effect "prestress" the longitudinal structural members of the former. Stresses on the main girder webs at the side spans were found to be the greatest.

Overall, the critical position of explicit Type RA1 loading was determined to be at 27 m (Fig. 17), corresponding approximately to both the maximum stress and the maximum out-of-plane displacement of the main girder top flanges.

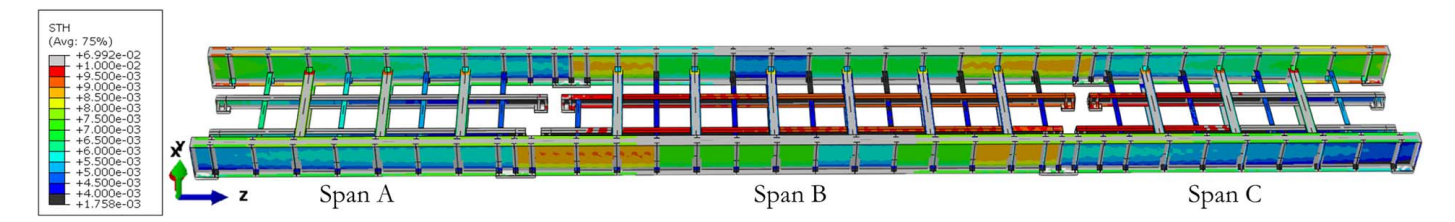


Fig. 16. Contour plot of typical nonuniformly corroded cross-sectional wall thicknesses on the case study bridge. This example shows the bridge at an age of 195 years, with the color spectrum corresponding to thicknesses ranging from 4 to 10 mm. Note: Color is used to quantitatively demonstrate that here the main girder webs are assigned with random spatial distribution of thickness, shown by the wave patterns on both girders.

Table 1. Magnitude of stress- and displacement-based bridge responses and the corresponding explicit Type RA1 train position, measured from the point at which the train enters the bridge

Potential failure modes	Span A	Span B	Span C
Maximum stress			_
On webs (main girders and rail bearers)	150 GPa @ 27 m	100 GPa @ 44 m	140 GPa @ 33 m
On flanges (main girders)	75 GPa @ 7 m	94 GPa @ 24 m	62 GPa @ 50 m
On bearing stiffeners (main girder)	43 GPa @ 43 m	32 GPa @ 42 m	42 GPa @ 51 m
Out-of-plane deflection (ratio to span length)	_	_	_
On top-flanges (main girders)	0.030% @ 26 m	0.019% @ 18 m	0.028% @ 52 m

Note: The bold values indicate the critical responses and the corresponding train positions.

Probabilistic Assessment Procedure

Latin Hypercube Sampling

Model uncertainties can have an important influence on the assessment of structural performance (Wilkie and Galasso 2020). Hence, the stochastic assignment of model parameters was employed, and the uncertainties were considered explicitly. Latin hypercube sampling was employed to improve sampling efficiency and quality. This technique is based on the idea of stratified sampling (Jones et al. 2002), which allows the analyst to have full control of both the statistical distribution and the statistical correlation of the generated samples. The number of Latin hypercube sampled realizations, n, equals the number of simulations required in the subsequent structural vulnerability assessment per age. The value of n must be sufficiently large such that the finite number of samples can be regarded as representative of the entire population. This could be verified by conducting a convergence analysis, although

herein, n = 30, as recommended by ASCE (2017) for safety-related nuclear structures subjected to seismic hazards, was considered to suffice and was adopted without further verification.

The stochastically sampled random model parameters are summarized in Table 2. Four categories of parameters are included: bridge material properties, bridge boundary conditions, nominal corrosion depths, and corrosion nonuniformity parameters. Statistical distribution types and parameters were taken from the literature when possible. The yield strength $f_{y,\text{steel}}$ and elastic modulus E_{steel} of early steel were treated as random variables, with nominal values from Kossakowski (2021) and their statistical distribution type and parameters from Hess et al. (2002). Variability of bridge boundary conditions was considered by altering the elastic modulus of the equivalent bridge bearings E_{bearing} . Given a lack of data, its statistical dispersion was assumed to be the same as that of E_{steel} . Corrosion in each zone was governed by two sets of random parameters: the nominal corrosion depths d_n (controlling temporal evolution) and a set of beta distribution parameters, α and β

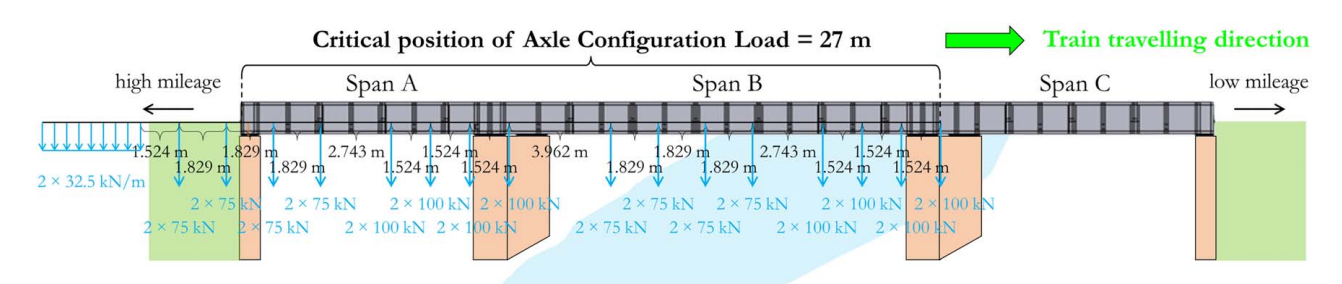


Fig. 17. Critically positioned Type RA1 loading referred to as the ALC in subsequent probabilistic analyses.

Table 2. List of stochastically sampled model parameters and values

Variable type	Symbol and description of a random variable	Statistical distribution	Nominal value N	Distribution parameters ^a			
Bridge materi	Bridge material						
$f_{y,\text{steel}}$	Early steel yield strength	Lognormal	$239 \times 10^3 \text{ kPa}$	$\mu = \log(N)$	$\sigma = 0.05$		
$E_{ m steel}$	Early steel elastic modulus	Normal	$190 \times 10^{6} \text{ kPa}$	$\mu = 0.987N$	$\sigma = 0.076 \mu$		
Boundary conditions							
$E_{ m bearing}$	Bearing elastic modulus	Normal	6,000 kPa	$\mu = N$	σ = 0.076 μ		
Nominal corrosion depth d_n (this is repeated for each corrosion zone)							
d_n	Nominal (maximum) double-side corrosion depth of each corrosion zone	Lognormal	Age-dependent, as described in Fig. 7(b)	$\mu = \log(\text{mean})$	σ = sigma		
Corrosion nonuniformity parameters (these are repeated for each corrosion zone)							
$lpha_1$	Beta distribution parameter α on Axis 1 (x- or y-axis)	Uniform	N/A	Lower = 0.5	Upper = 1.2		
$oldsymbol{eta}_1$	Beta distribution parameter β on Axis 1 (x- or y-axis)	Uniform	N/A	Lower = 0.5	Upper = 1.2		
α_2	Beta distribution parameter α on Axis 2 (z-axis)	Uniform	N/A	Lower = 0.8	Upper $= 1.5$		
eta_2	Beta distribution parameter β on Axis 2 (z-axis)	Uniform	N/A	Lower = 0.8	Upper = 1.5		

 $^{^{}a}\mu$ denotes the mean value for normal distribution or the mean of logarithmic values for lognormal distribution. σ denotes the standard deviation for normal distribution or the standard deviation of logarithmic values for lognormal distribution. For uniform distribution, the distribution parameters are upper and lower bounds.

(controlling spatial distribution). Corrosion depths d_n were age-dependent, following the corrosion model described in Fig. 7(b). The beta distribution parameters, α and β , were sampled as uniformly distributed variables with specified ranges. A correlation coefficient of 0.8 was assigned to each pair of α and β parameters. All other model parameters were assumed to have zero statistical correlation with each other.

Nonlinear Static Instability (Riks) Analysis

When there is the potential for severe geometric nonlinearity in the finite-element model, negative stiffness may be present in the loaddisplacement response, and the structure must release strain energy to remain in equilibrium (SIMULIA 2014). Given this, unstable collapse and postbuckling analysis must be carried out for each of the Latin hypercube sampled realizations, instead of using the standard static analysis procedure. The Riks method (SIMULIA 2014) in Abaqus was used. The method is suitable for finding static equilibrium states when there are concerns regarding material nonlinearity, prebuckling geometric nonlinearity, or unstable postbuckling responses. During a Riks analysis, the applied load is treated as an unknown and is solved simultaneously with the other responses. Progress of the numerical solution is measured not by pseudotime but arc length, and the load magnitude is allowed to change nonmonotonically as the analysis progresses. A reference load should be prescribed and is proportionally ramped from the initial state. The following Riks analysis termination criteria were adopted:

- 1. Load proportionality factor = 1.5 (sufficiently large to cover the largest possible train load with some extra margin to produce the data necessary for vulnerability analysis).
- 2. Maximum out-of-plane displacement of the main girder upper flange and web plates = 20 mm (a value large enough to guarantee the occurrence of girder buckling).
- 3. Completion of a sufficient number of analysis steps (to avoid sustained analysis time of any one case).

Multiple termination criteria were employed simultaneously. This was because the targeted load proportionality factor might never be reached in some scenarios due to an early onset of buckling, whereas in other scenarios, buckling may never occur. The Riks method only works well in the absence of potential bifurcation (Houliara and Karamanos 2011). This can be ensured by introducing small imperfections to the model, such as the localized wall thickness nonuniformity as defined in Eq. (7), or a small perturbation force at the center of the top flanges of the main girders.

During each nonlinear static analysis, train loads were applied as pushover forces, increasing from zero to a large value. The maximum load magnitude was sufficiently larger than the largest possible train load of interest, so as to accommodate appropriate curve fitting processes (Zhang et al. 2023) during the subsequent structural vulnerability analysis.

Structural Vulnerability Analysis

Structural vulnerability assessment was carried out following an approach similar to that proposed in Baker (2015) to derive fragility

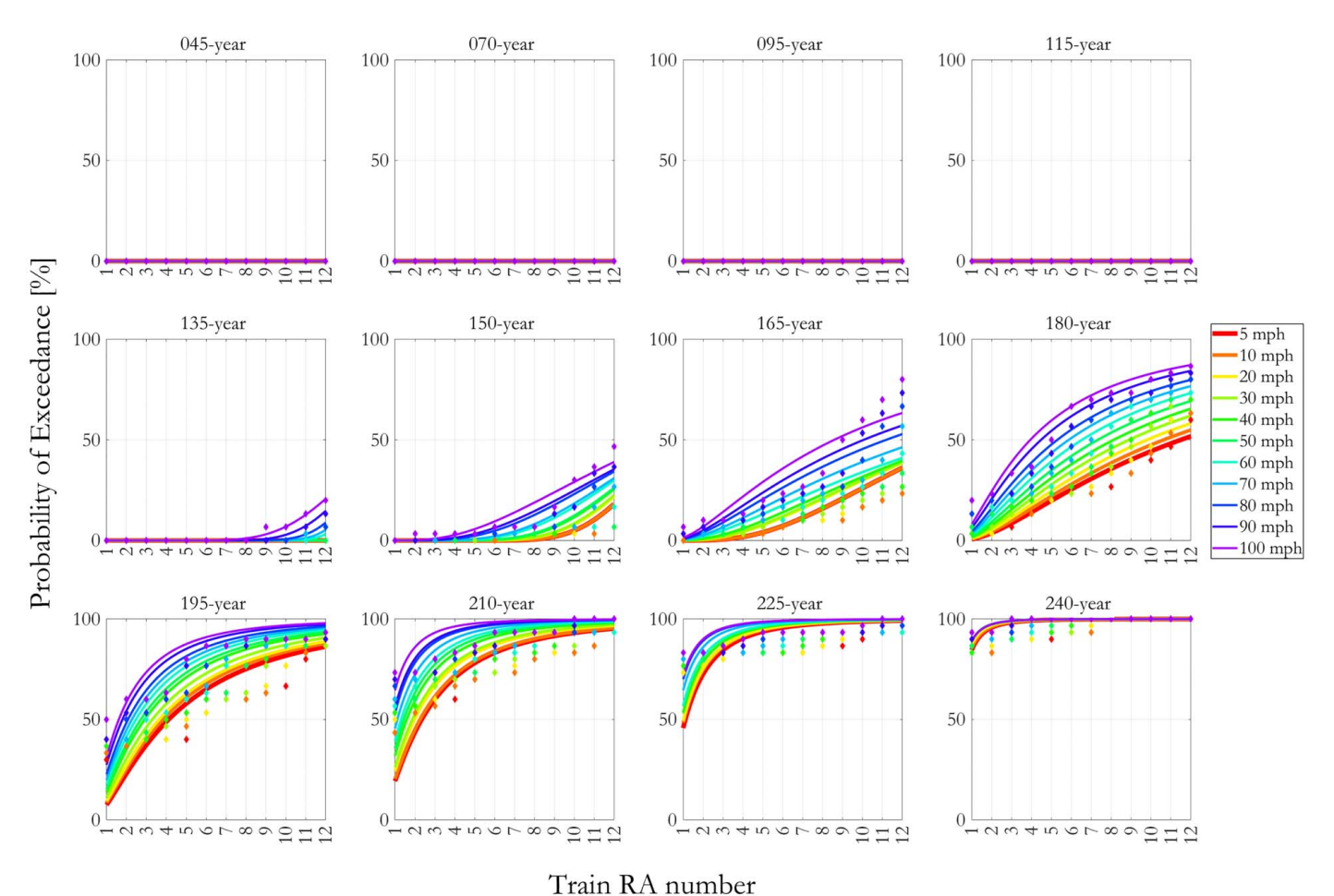


Fig. 18. Fragility functions of the case study bridge subjected to ELC.

functions in the field of earthquake engineering, that is, the probability of exceeding a damage measure threshold as a function of a ground motion intensity measure. In this case, in place of the seismic ground motion intensity commonly seen in the literature, HAW train load is regarded as a hazard that the structure needs to withstand, and the train RA number is the intensity measure. A fragility function takes the mathematical form of a lognormal cumulative distribution function:

$$P(DM_i|RA = x) = \Phi\left(\frac{\ln(x/\theta)}{\beta}\right)$$
 (12)

where $P(\mathrm{DM}_i|\mathrm{RA}=x)=$ probability that train load at RA number = x (with a fixed train speed) leads to the exceedance of a damage measure threshold; $\Phi()=$ standard normal cumulative distribution function; $\theta=$ median value of the fragility function to be estimated (i.e., the train RA number level corresponding to 50% probability of exceedance); and $\beta=$ logarithmic standard deviation of ln(RA) to be estimated. Eq. (12) assumes that, at a certain bridge age, the train loads that can lead to the exceedance of a damage measure threshold are lognormally distributed. This assumption is common in structural vulnerability assessments (Gernay et al. 2019; McKenna et al. 2021). Parameters θ and β are estimated based on structural analysis results.

Assuming the results of all analysis cases (exceedance or non-exceedance of failure criteria) are statistically independent from each other, the probability of observing z_i exceedances out of a

total number of $n_j = n = 30$ analysis will follow a binomial distribution:

$$P(z_j \text{ exceedances in } n_j \text{ realisations}) = \binom{n_j}{z_j} p_j^{z_j} (1 - p_j)^{n_j - z_j} \quad (13)$$

where p_j = probability that an analysis case leads to the exceedance of a damage measure threshold at a particular train RA number = x_j ; and the subscript, j = 1 to m, denotes the sequence of train RA numbers examined, RA0–RA12. To determine the fragility function, which predicts p_j , the maximum likelihood method (Shinozuka et al. 2000) is used to estimate θ and β values that best fit the observation data. When analysis data are obtained for multiple train RA levels, the product of binomial probabilities obtained from Eq. (13) at each train RA level, 1 to m, can be summarized as the likelihood of the entire data set:

Likelihood =
$$\prod_{j=1}^{m} {n_j \choose z_j} p_j^{z_j} (1 - p_j)^{n_j - z_j}$$
 (14)

where m = total number of train RA numbers considered; and $\Pi =$ multiplication over all train RA numbers. Eq. (14) can be rewritten by substituting p_i using the expression in Eq. (12), as follows:

Likelihood =
$$\prod_{j=1}^{m} {n_j \choose z_j} \Phi\left(\frac{\ln(x_j/\theta)}{\beta}\right)^{z_j} \left[1 - \Phi\left(\frac{\ln(x_j/\theta)}{\beta}\right)\right]^{n_j - z_j}$$
(15)

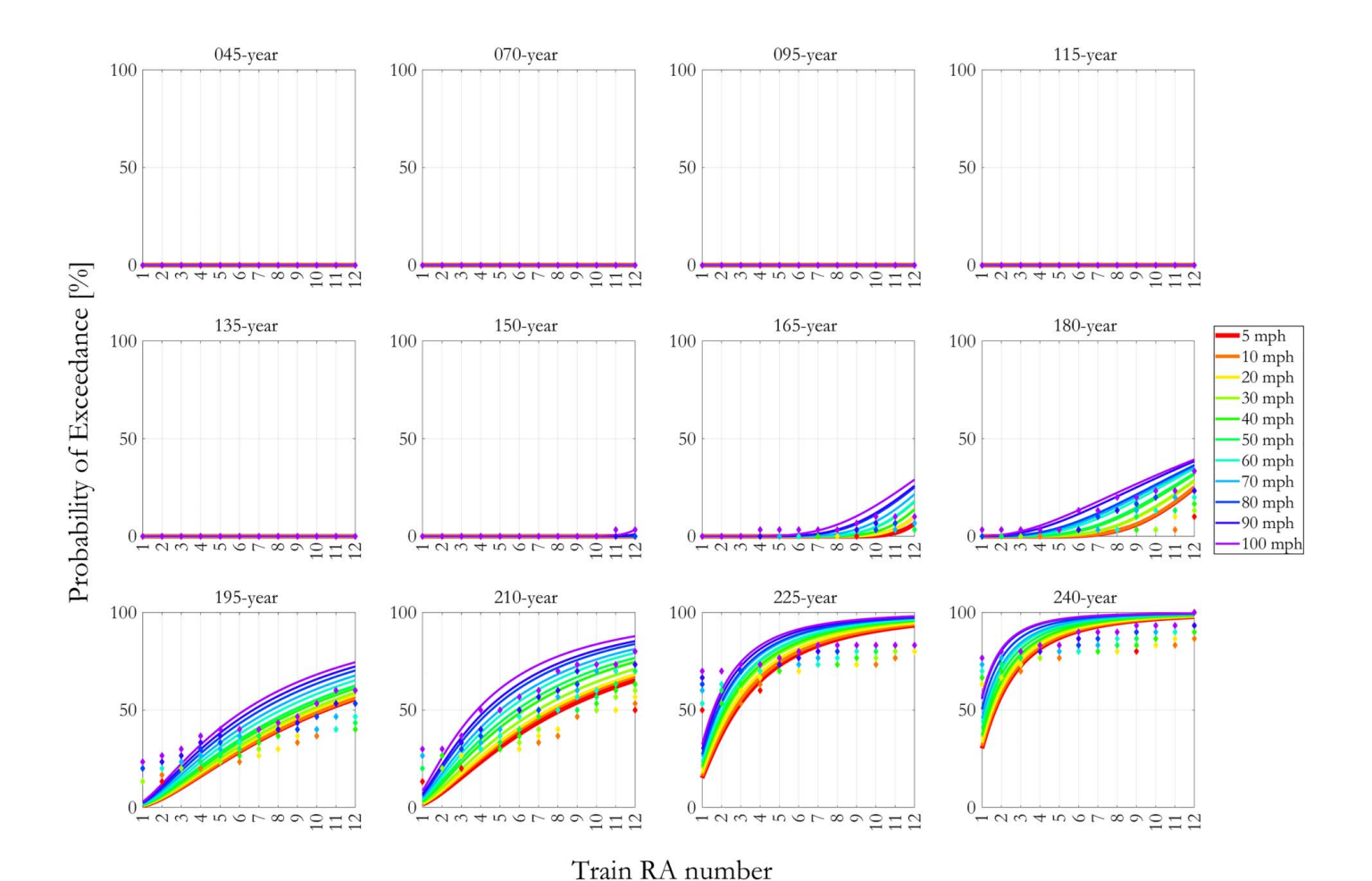


Fig. 19. Fragility functions of the case study bridge subjected to ALC.

Estimates of fragility function parameters, $\hat{\vartheta}$ and $\hat{\beta}$, can then be obtained by maximizing this likelihood function:

$$\{\hat{\theta}, \hat{\beta}\} = \underset{\theta, \beta}{\operatorname{argmax}} \sum_{j=1}^{m} \left\{ \ln \binom{n_{j}}{z_{j}} + z_{j} \ln \Phi \left(\frac{\ln(x_{j}/\theta)}{\beta} \right) + (n_{j} - z_{j}) \ln \left[1 - \Phi \left(\frac{\ln(x_{j}/\theta)}{\beta} \right) \right] \right\}$$
(16)

This process produces a single fragility curve as in Eq. (12). The calculation should be carried out repeatedly for different bridge ages and permissible train speeds. This gives a suite of age- and speed-dependent fragility functions.

Subsequently, estimates of future bridge capacity are determined based on the suite of fragility functions and a prescribed confidence level, for example, 95%. The highest train RA number satisfying the prescribed confidence level can be identified for each age- and speed-dependent fragility function, as floating-point numbers to carry out this calculation. For each bridge age, regression analyses can then be undertaken to fit these speed-dependent data points to an appropriate function, such as a power function, to produce BDEs:

$$RA(v) = p_1 v^{p_2} < 10 (17)$$

where RA(v) = estimated bridge RA number (integer) as a function of a permissible train speed v; p_1 and p_2 = regression coefficients to be estimated; and $\lfloor \rfloor$ = floor function, which takes a real number as input and gives the greatest integer less than or equal to that number as output. Estimates of bridge RA capacity are given up to RA10 and BDEs can be calculated repeatedly for different bridge ages of interest.

Probabilistically Estimated Age- and Speed-Dependent Future Route Availability of the Case Study Bridge Subjected to Different Load Configurations

Age- and Speed-Dependent Bridge Fragility Curves

The fraction of exceedance cases for each damage measure threshold can be counted at load magnitudes corresponding to each train RA number, permissible speed, and bridge age. For estimating BDEs for the case study bridge, the exceedance of any one of the four damage measure thresholds was considered as the point of onset of overall structural failure. The corresponding applied train load was thus considered as an estimate of residual bridge capacity, which was subsequently used in the structural vulnerability analysis.

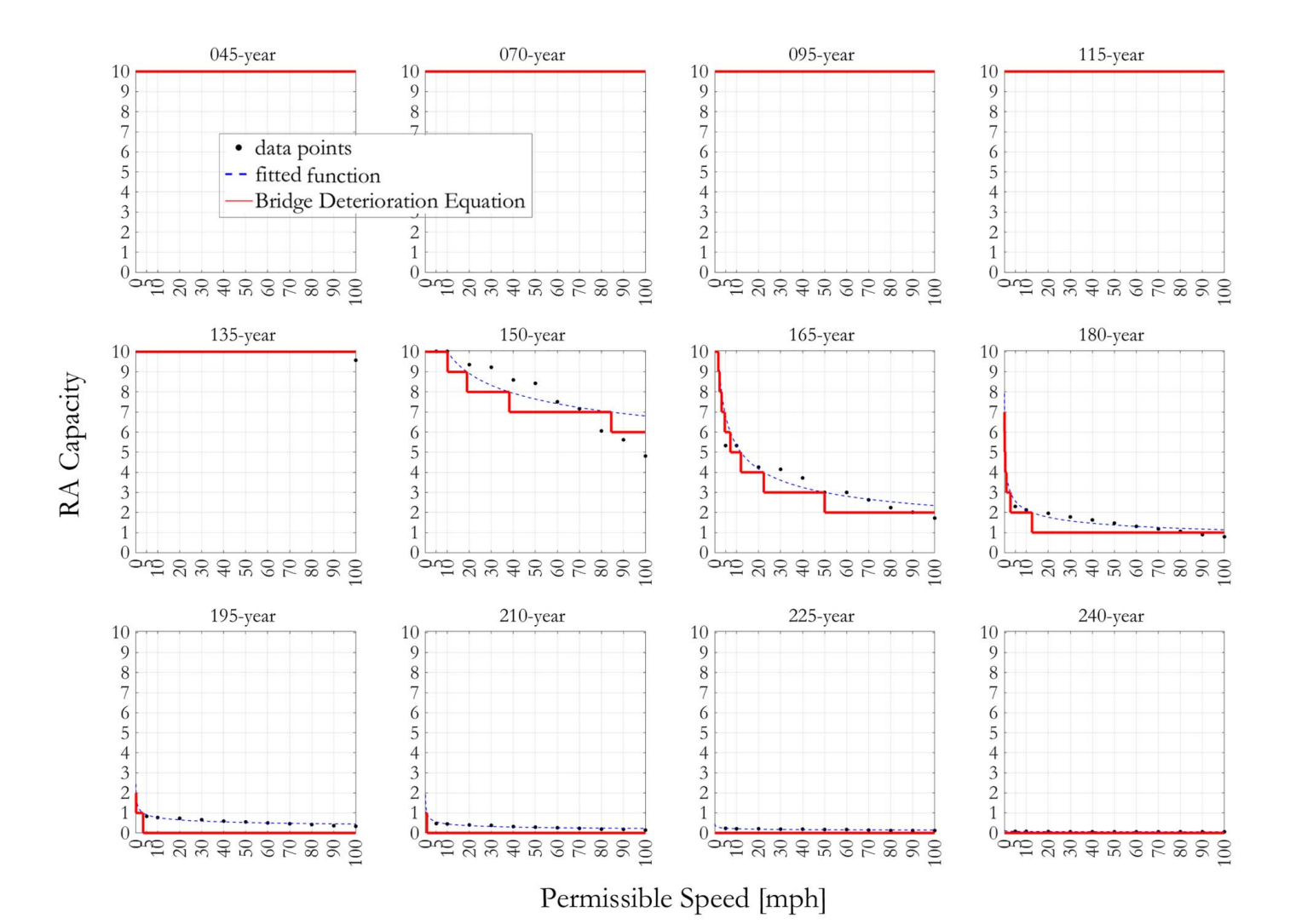


Fig. 20. BDEs of the case study bridge subjected to ELC given a 95% confidence level.

Age- and speed-dependent fragility curves are presented in Figs. 18 and 19 for the case study bridge subjected to ELC and ALC loads, respectively. Under ELC train load, the fitted fragility curves suggest that the probability of exceeding any one of the damage measure thresholds is negligible up to an age of 115 years, for trains up to RA12 at speeds up to 100 mi/h. Nonzero probabilities of exceedance are calculated when the age of the bridge is over 135 years, in which the probability of exceedance is greater if either the axle weight or the speed of the train on the bridge is higher. Moreover, bridge fragility only has limited variability with respect to different train speeds at any particular age. Beyond an age of 195 years, the probability of exceeding any damage measure thresholds reaches approximately 10% even for RA1 trains traveling at only 5 mi/h.

When subjected to ALC train load, nonnegligible probabilities of exceeding any damage measure threshold do not occur until 165 years, and the derived fragility curves, overall, show lower probabilities of exceedance for the same levels of train RA number and permissible speed than the ELC. This might be attributed to the fact that for the same train RA number, the total force applied on the bridge is greater in the ELC than in the ALC. Comparison of Fig. 18 with Fig. 19 shows that an additional approximately 30 years of bridge service life can be extracted for the case study bridge if the analysis is carried out using ALC rather than ELC.

This demonstrates how different modeling assumptions may significantly affect the results, further highlighting the fact that numerical estimations should be regarded as supplementary information, to be used in conjunction with appropriate site inspection and engineering judgment in any decision-making process.

Estimated BDE

BDEs are given in Figs. 20 and 21 for the case study bridge subjected to ELC and ALC loads, respectively, assuming a 95% confidence level. For ELC, the estimated BDEs suggest the bridge can be rated at RA10 for all train speeds up to an age of 135 years. The bridge RA number reduces with increasing age—more rapidly for faster train speeds, in line with engineering judgment. At an age of 165 years, the bridge route availability is reduced to RA6 at 5 mi/h or RA5 at 10 mi/h. The ELC load is the more conservative configuration. Under ALC loading, the bridge is rated RA10 for all train speeds up to 150 years of age and has minimal capacity up to 195 years without any intervention measures.

To accommodate the estimated permissible train RA number at various speeds, restrictions in terms of either or both factors can be imposed on the bridge as needed. At certain ages, trains with higher RA numbers can be permitted to cross the bridge by imposing stricter speed restrictions. For example, assuming

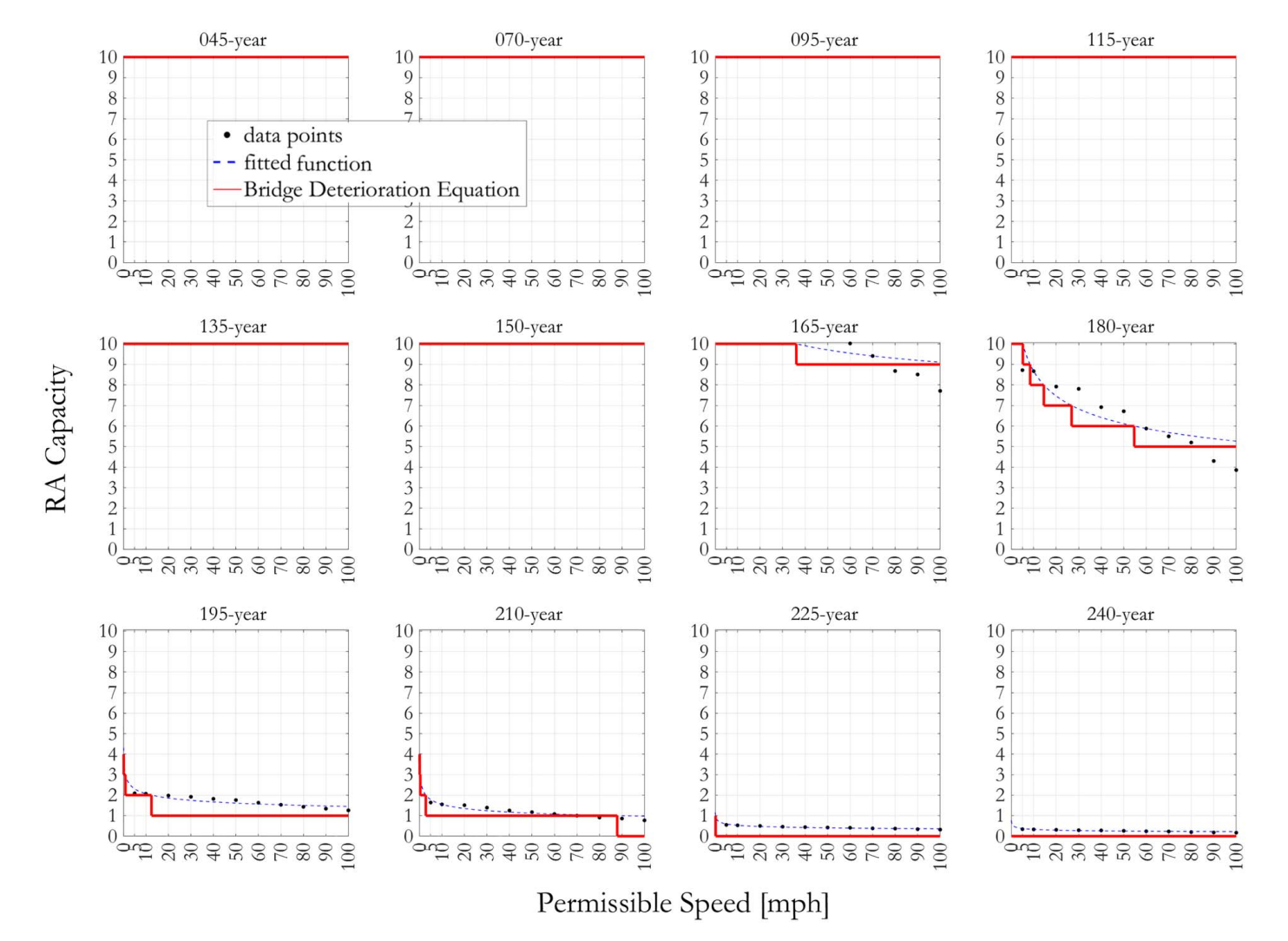


Fig. 21. BDEs of the case study bridge subjected to ALC given a 95% confidence level.

ELC train load at 150 years of age, the bridge is rated RA6 up to 100 mi/h, increasing to RA8 if a 30 mi/h speed limit is imposed, or to RA10 if the train speed is limited to 10 mi/h. At 165 years of age, the RA capacity is only RA3 for a train traveling at 50 mi/h, but can be increased to RA6 with a speed restriction of 5 mi/h. This would at least allow certain trains to pass through the route while the bridge is waiting to be retrofitted or replaced. Nonetheless, as the bridge further deteriorates, imposing stricter speed restrictions would not have much effect because the assessed capacity is already low under near-static loading conditions.

The highly nonlinear impact of corrosion on bridge performance can be attributed to three factors. The first is the nonlinear development of corrosion depth versus age adopted on this bridge [Fig. 7(b)]. Second, even if the rate of corrosion were to be considered constant (so that the corroded plate thicknesses reduced linearly with age), degradation of structural capacity over time would still likely be nonlinear. According to Kirchhoff's thin plate theory, the critical buckling load of thin rectangular plates is proportional to their flexural rigidity, which depends on plate thickness via a cubic term (Reddy 2006). The macroscopic nonuniformity of corrosion distribution is also a likely contributing factor to the nonlinear degradation of bridge performance. The distribution determines the state/location of the worst corroded portion on a bridge and thus influences the interaction between various failure (especially buckling) modes and their relative criticality, among which some are more detrimental than others owing to insufficient capacity reserve after failure initiation. Therefore, although the initial process of corrosion might appear slow, its effects on structural performance may disproportionately increase as time goes on. It is thus recommended that metallic railway bridges be repainted at regular intervals to prevent the initiation or reduce the rate of corrosion.

Conclusions

Currently, HAW trains designated RA9 and RA10 are permitted to travel on UK railways only with specific dispensations, which could in theory be withdrawn if the RA rating of the bridge drops below that of the freight consist, resulting in significant economic losses to both the railway infrastructure owner and freight operators. It is therefore necessary to understand the impact of HAW trains on old railway bridges and to estimate their future route availability. To this end, a probabilistic assessment framework for estimating the future load carrying capacity of aging metallic railway bridges is proposed. The framework is demonstrated through a case study analysis of a typical three-span, 37.7-m-long, half-through, early steel railway bridge built in 1903. Nonlinear responses of the bridge when subjected to HAW train loads are evaluated using advanced numerical models that account for buckling and unstable collapse. Possible structural failure mechanisms of the bridge are explored using suitable damage measures related to both global and localized structural performance. Aging of the metallic bridge is modeled assuming that deterioration occurred primarily by time-dependent corrosion. Various model uncertainties, including those governing the long-term temporal evolution and macroscopic spatial distribution of corrosion depth, are explicitly accounted for by sampling multiple realizations from a set of predefined multivariate statistical distributions. A suite of BDEs is produced, which estimates bridge RA capacity as a function of bridge age and permissible train speed. The BDE formulation provides a straightforward piece of information, valuable in potential

data-driven decision-making processes. Key findings are summarized as follows:

- The derived BDE suggests that the bridge at present age (121 years) provides sufficient access to HAW traffic despite suffering from noticeable corrosion-induced cross-sectional losses distributed across all metallic parts, with the maximum corrosion depth taken as 3 mm based on the immediately preceding inspection. Calculated natural frequencies for vertical vibration modes were 6.5 and 11.2 Hz for the center span and the two side spans, respectively.
- 2. With the adopted corrosion model, the RA capacity of the bridge is anticipated to deteriorate quickly if no intervention measures are provided. At a bridge age of approximately 150 years, speed restrictions will need to be imposed to provide continued safe access to HAW trains, with the bridge rated RA8 at 30 mi/h, RA9 at 20 mi/h, and RA10 at 10 mi/h. At the age of 180 years, the bridge will be unable to provide access to any trains at all. This result depends on the assumed corrosion models, which govern both the temporal evolution and spatial distributions of corrosion depth. The increasingly disproportionate impact of corrosion on structural capacity is not only attributed to the nonlinearity in the corrosion model itself, but the dependency of the critical buckling load of Kirchhoff's thin plates on the cube of the plate thickness.
- 3. The adopted modeling assumptions must be carefully verified before the analyses. This study demonstrates this by comparing the results derived on the basis of two different train load idealizations: the more rudimentary ELC and the more elaborate moving ALCs. Due to its simplified nature, the ELC turns out to be more conservative and results in an estimated bridge service life 30 years less than that using ALC.
- 4. The most critical loading scenario under quasi-static ALC loading is not when all three spans of the bridge are fully loaded but when the bridge is loaded on only the first two spans, with no external force acting on the third.

The present study also identified several aspects toward which future works can be directed:

- A major aspect of uncertainty in estimating future bridge capacity is the identification of appropriate corrosion models for both long-term temporal evolution and macroscopic spatial distribution. There is a need for future research on reliable corrosion models that are applicable for the typical material and structural types of aging metallic bridges.
- 2. Future research is also needed to improve the method for quantifying various buckling classes on U-frame metallic bridges, and to facilitate fully automated identification. This extends to other bridge types as well, if the proposed framework is to be repeated to produce BDE for a large number of other bridges.
- 3. Future research can also usefully incorporate the following aspects to improve the integrity of the estimation: other valid aging pathways such as fatigue, material creep, or foundation degradation; individual intervention measures such as coating repairs or structural retrofitting; and complex interactive mechanisms such as fatigue corrosion.
- 4. The derivation of BDE involves a manually conducted desk study, numerical simulations, and postprocessing procedures that are specific to individual bridges, with scope for the analyst to decide how advanced or idealized the simulations might be. Future studies could thus usefully focus on the development and verification of a simplified, yet accurate, generalized numerical modeling approach that will reduce the required analysis time in the context of producing BDE for all bridges along a railway route and ultimately moving toward, for example, the

development of a set of data-driven surrogate models (Lei et al. 2024) that supplies estimated BDEs of a large number of bridges to an expert online geodatabase, which is an ongoing work (Armstrong et al. 2025), for making quick estimations of future load carrying capacity of aging metallic railway bridges on a route/network level.

Data Availability Statement

The data sets generated during and/or analyzed during the current study are available from the corresponding author upon reasonable request. Some data, models, or code generated or used during the study are proprietary or confidential in nature and may only be provided with restrictions (data related to the identity of the studied bridge are confidential).

Acknowledgments

This study was part of a research project sponsored and funded by the UK Rail Safety and Standards Board (RSSB) and Network Rail [Development of a prototype Heavy Axle Weight modeling tool (T1300)]. The authors are grateful for the input and support provided by colleagues and collaborators across the research project, notably at RSSB and Network Rail. The authors would also like to thank Rod Anderson, John Armstrong, Simon Blainey, Saba Ghassemi, John Harkness, and Jason Sadler (listed in alphabetical order) of the University of Southampton for their involvement in this research project.

Author contributions: All authors contributed to the study and approved the final manuscript. Ziliang Zhang: Conceptualization, Methodology, Software, Formal analysis, Data curation, Writing—original draft preparation and Visualization. Geoff Watson: Conceptualization, Investigation, Resources, Writing—review and editing and Project administration. David Milne: Investigation and Writing—review and editing. William Powrie: Conceptualization, Writing—review and editing, Supervision, Project administration and Funding acquisition. Mohammad M. Kashani: Conceptualization, Methodology, Writing—review and editing, and Supervision.

References

- Abbas, M., and M. Shafiee. 2020. "An overview of maintenance management strategies for corroded steel structures in extreme marine environments." *Mar. Struct.* 71: 102718. https://doi.org/10.1016/j.marstruc.2020.102718.
- Adams, T. M., and M. Kang. 2009. Sensitivity of bridge health index to element failure costs and conditions. Rep. No. MRUTC 08-07. Washington, DC: Transportation Research Board.
- Ádány, S., A. L. Joó, and B. W. Schafer. 2010. "Buckling mode identification of thin-walled members by using cFSM base functions." Thin-Walled Struct. 48 (10–11): 806–817. https://doi.org/10.1016/j.tws.2010.04.014.
- Ahola, A., K. Lipiäinen, S. Afkhami, H. Lilja, and T. Björk. 2022. "Fatigue performance of the welded details of an old, demolished steel railway bridge." *Eng. Struct.* 256: 113966. https://doi.org/10.1016/j.engstruct .2022.113966.
- Akgul, F. 2016. "Bridge management in Turkey: A BMS design with customised functionalities." Struct. Infrastruct. Eng. 12 (5): 647–666. https://doi.org/10.1080/15732479.2015.1035284.
- Armstrong, J., J. Sadler, S. Blainey, G. Watson, W. Powrie, M. Kashani, J. Harkness, Z. Zhang, and R. Anderson. 2025. "Modelling the interactions between heavy axle weight rail freight traffic and underbridges." In Proc., 11th Int. Conf. on Railway Operations Modelling and

- Analysis (RailDresden 2025). Dresden, Germany: TUD Dresden University of Technology.
- ASCE. 2017. Seismic analysis of safety-related nuclear structures, 1–171. Reston, VA: ASCE.
- Ataei, N., and J. E. Padgett. 2013. "Probabilistic modeling of bridge deck unseating during hurricane events." *J. Bridge Eng.* 18 (4): 275–286. https://doi.org/10.1061/(ASCE)BE.1943-5592.0000371.
- Bai, Y., Y. Kim, H.-b. Yan, X.-f. Song, and H. Jiang. 2015. "Reassessment of the jacket structure due to uniform corrosion damage." *Ships Offshore Struct.* 11 (1): 1–8. https://doi.org/10.1080/17445302.2015.1021139.
- Baker, J. W. 2015. "Efficient analytical fragility function fitting using dynamic structural analysis." *Earthquake Spectra* 31 (1): 579–599. https://doi.org/10.1193/021113EQS025M.
- Bolukbasi, M., J. Mohammadi, and D. Arditi. 2004. "Estimating the future condition of highway bridge components using national bridge inventory data." *Pract. Period. Struct. Des. Constr.* 9 (1): 16–25. https://doi.org/10.1061/(asce)1084-0680(2004)9:1(16).
- BSI (British Standards Institution). 2000. Steel, concrete and composite bridges—Part 3: Code of practice for design of steel bridges, 1–201. BS 5400-3:2000. London: BSI.
- Canning, L., and M. M. Kashani. 2016. "Assessment of U-type wrought iron railway bridges." *Proc. Inst. Civ. Eng. Eng. Hist. Heritage* 169 (2): 58–67. https://doi.org/10.1680/jenhh.15.00017.
- Clark, G. W. 1997. Route availability: Comparison of RA and RIS systems.Rep. No. RR-TCE-094. London, UK: Track and Civil Engineering Group, British Rail Research.
- Czarnecki, A. A., and A. S. Nowak. 2008. "Time-variant reliability profiles for steel girder bridges." *Struct. Saf.* 30 (1): 49–64. https://doi.org/10.1016/j.strusafe.2006.05.002.
- Darban, S., H. Ghasemzadeh Tehrani, and N. Karballaeezadeh. 2020. Presentation a New Method for Determining of Bridge Condition Index by Using Analytical Hierarchy Process, 1–13. Basel, Switzerland: MDPI.
- Dassault Systèmes. 2023. "Abaqus/Standard: Solution technology for linear and nonlinear finite element analysis." Accessed August 20, 2023. https://www.3ds.com/products-services/simulia/products/abaqus/abaqusstandard/
- Decker, J. B., K. M. Rollins, and J. C. Ellsworth. 2008. "Corrosion rate evaluation and prediction for piles based on long-term field performance." J. Geotech. Geoenviron. Eng. 134 (3): 341–351. https://doi .org/10.1061/(ASCE)1090-0241(2008)134:3(341).
- DeStefano, P. D., and D. A. Grivas. 1998. "Method for estimating transition probability in bridge deterioration models." *J. Infrastruct. Syst.* 4 (2): 56–62. https://doi.org/10.1061/(ASCE)1076-0342(1998)4:2(56).
- Dizaj, E. A., J. E. Padgett, and M. M. Kashani. 2021. "A Markov chain-based model for structural vulnerability assessment of corrosion-damaged reinforced concrete bridges." *Phil. Trans. R. Soc. A* 379 (2203): 20200290. https://doi.org/10.1098/rsta.2020.0290.
- DOT. 2016. Synthesis of national and international methodologies used for bridge health indices. Rep. No. FHWA-HRT-15-081. McLean, VA: DOT.
- FHWA (Federal Highway Administration). 2005. *Bridge management experiences of California, Florida, and South Dakota*. Rep. No. FHWA IF-05-040. Washington, DC: FHWA.
- Fisher, J. W., B. T. Yen, and D. Wang. 1990. "Fatigue strength of riveted bridge members." *J. Struct. Eng.* 116 (11): 2968–2981. https://doi.org/10.1061/(ASCE)0733-9445(1990)116:11(2968).
- Garbatov, Y., and C. Guedes Soares. 2008. "Corrosion wastage modeling of deteriorated bulk carrier decks." *Int. Shipbuild. Prog.* 55 (1–2): 109– 125. https://doi.org/10.3233/ISP-2008-0041.
- Gernay, T., N. E. Khorasani, and M. Garlock. 2019. "Fire fragility functions for steel frame buildings: Sensitivity analysis and reliability framework." Fire Technol. 55 (4): 1175–1210. https://doi.org/10.1007/s10694-018-0764-5.
- Gong, C., and D. M. Frangopol. 2020. "Reliability of steel girder bridges with dependent corrosion growth." *Eng. Struct.* 224: 111125. https:// doi.org/10.1016/j.engstruct.2020.111125.
- Gu, G., A. Kapoor, and D. M. Lilley. 2008. "Calculation of dynamic impact loads for railway bridges using a direct integration method." Proc. Inst.

- *Mech. Eng., Part F: J. Rail Rapid Transit* 222: 385–398. https://doi.org/10.1243/09544097JRRT189.
- Han, D., and W. Che. 2021. "Comparison of the shear modulus of an offshore elastomeric bearing between numerical simulation and experiment." Appl. Sci. 11 (10): 4384. https://doi.org/10.3390/ app11104384.
- Han, X., D. Y. Yang, and D. M. Frangopol. 2019. "Time-variant reliability analysis of steel plates in marine environments considering pit nucleation and propagation." *Probab. Eng. Mech.* 57: 32–42. https://doi. org/10.1016/j.probengmech.2019.05.003.
- Hess, P. E., D. Bruchman, I. A. Assakkaf, and B. M. Ayyub. 2002. "Uncertainties in material and geometric strength and load variables." Nav. Eng. J. 114 (2): 139–166. https://doi.org/10.1111/j.1559-3584 .2002.tb00128.x.
- Houliara, S., and S. A. Karamanos. 2011. "Buckling of thin-walled long steel cylinders subjected to bending." J. Pressure Vessel Technol. 133 (1): 011201. https://doi.org/10.1115/1.4002902.
- Imam, B. M., and M. K. Chryssanthopoulos. 2012. "Causes and consequences of metallic bridge failures." Struct. Eng. Int. 22 (1): 93–98. https://doi.org/10.2749/101686612X13216060213437.
- Imam, B. M., and T. D. Righiniotis. 2010. "Fatigue evaluation of riveted railway bridges through global and local analysis." *J. Constr. Steel Res.* 66 (11): 1411–1421. https://doi.org/10.1016/j.jcsr.2010.04.015.
- Jones, A. L., S. L. Kramer, and P. Arduino. 2002. Estimation of uncertainty in geotechnical properties for performance-based earthquake engineering. Berkeley, CA: Pacific Earthquake Engineering Research Center, Univ. of California.
- Khandel, O., and M. Soliman. 2021. "Integrated framework for assessment of time-variant flood fragility of bridges using deep learning neural networks." J. Infrastruct. Syst. 27 (1): 1–16. https://doi.org/10.1061/ (ASCE)IS.1943-555X.0000587.
- Khodabux, W., P. Causon, and F. Brennan. 2020. "Profiling corrosion rates for offshore wind turbines with depth in the north sea." *Energies* 13 (10): 2518. https://doi.org/10.3390/en13102518.
- Kossakowski, P. G. 2021. "Mechanical properties of bridge steel from the late 19th century." Appl. Sci. 11 (2): 478. https://doi.org/10.3390/ app11020478.
- Kowal, M., and M. Szala. 2020. "Diagnosis of the microstructural and mechanical properties of over century-old steel railway bridge components." Eng. Fail. Anal. 110: 104447. https://doi.org/10.1016/j.engfailanal.2020.104447.
- Le, B., and J. Andrews. 2013. "Modelling railway bridge asset management." *Proc. Inst. Mech. Eng., Part F: J. Rail Rapid Transit* 227 (6): 644–656. https://doi.org/10.1177/0954409713490924.
- Lei, X., R. Feng, Y. Dong, and C. Zhai. 2024. "Bayesian-optimized interpretable surrogate model for seismic demand prediction of urban highway bridges." *Eng. Struct.* 301: 117307. https://doi.org/10.1016/j.engstruct.2023.117307.
- LoBEG (London Bridges Engineering Group). 2010. Bridge condition indicators project: Structures condition survey of borough principal road network, six year report—April 03 to March 09. London: LoBEG
- Macho, M., P. Ryjáček, and J. Matos. 2019. "Fatigue life analysis of steel riveted rail bridges affected by corrosion." *Struct. Eng. Int.* 29 (4): 551– 562. https://doi.org/10.1080/10168664.2019.1612315.
- Madanat, S., R. Mishalani, and W. H. W. Ibrahim. 1995. "Estimation of infrastructure transition probabilities from condition rating data." J. Infrastruct. Syst. 1 (2): 120–125. https://doi.org/10.1061/(ASCE) 1076-0342(1995)1:2(120).
- Martland, C. D. 2013. "Introduction of heavy axle loads by the north American rail industry." *J. Transp. Res. Forum* 52 (2): 103–125. https://doi.org/10.22004/ag.econ.207349.
- MathWorks. 2023. Matlab R2023a. Natick, MA: MathWorks.
- Mauch, M., and S. Madanat. 2001. "Semiparametric hazard rate models of reinforced concrete bridge deck deterioration." *J. Infrastruct. Syst.* 7 (2): 49–57. https://doi.org/10.1061/(asce)1076-0342(2001)7:2(49).
- McKenna, G., S. A. Argyroudis, M. G. Winter, and S. A. Mitoulis. 2021. "Multiple hazard fragility analysis for granular highway embankments: Moisture ingress and scour." *Transp. Geotech.* 26: 100431. https://doi.org/10.1016/j.trgeo.2020.100431.

- Melchers, R. E. 1999. "Corrosion uncertainty modelling for steel structures." J. Constr. Steel Res. 52 (1): 3–19. https://doi.org/10.1016/S0143-974X(99)00010-3.
- Melchers, R. E. 2003a. "Probabilistic models for corrosion in structural reliability assessment—Part 2: Models based on mechanics." J. Offshore Mech. Arct. Eng. 125 (4): 272–280. https://doi.org/10.1115/1.1600468.
- Melchers, R. E. 2003b. "Probabilistic models for corrosion in structural reliability assessment—Part 1: Empirical models." J. Offshore Mech. Arct. Eng. 125 (4): 264–271. https://doi.org/10 .1115/1.1600467.
- Melchers, R. E. 2018. "Progress in developing realistic corrosion models." Struct. Infrastruct. Eng. 14 (7): 843–853. https://doi.org/10.1080/ 15732479.2018.1436570.
- Melchers, R. E., and R. Emslie. 2016. "Investigations for structural safety assessment of corroded cast iron bridge piers." *Aust. J. Struct. Eng.* 17 (1): 55–66. https://doi.org/10.1080/13287982.2015.1128379.
- MHURD (China Ministry of Housing and Urban-Rural Development). 2003. *Technical code of maintenance for city bridge*, 1–147. [In Chinese.] Beijing: MHURD.
- Morcous, G., H. Rivard, and A. M. Hanna. 2002. "Modeling bridge deterioration using case-based reasoning." *J. Infrastruct. Syst.* 8 (3): 86–95. https://doi.org/10.1061/(ASCE)1076-0342(2002)8:3(86).
- Moy, S. S. J., H. W. J. Clarke, and S. R. Bright. 2009. "The engineering properties of Victorian structural wrought iron." *Proc. Inst. Civ. Eng. Constr. Mater.* 162 (1): 1–10. https://doi.org/10.1680/coma.2009 .162.1.1.
- Nakamura, S., T. Ogata, M. Takano, and Y. Kobayashi. 2019. "New technologies in retrofitting and strengthening of ageing steel and composite bridges in Japan." *Struct. Eng. Int.* 29 (4): 519–526. https://doi.org/10.1080/10168664.2019.1628618.
- Nedelcu, M., and H. L. Cucu. 2014. "Buckling modes identification from FEA of thin-walled members using only GBT cross-sectional deformation modes." *Thin-Walled Struct*. 81: 150–158. https://doi.org/10.1016/j .tws.2013.06.007.
- Network Rail. 2006. The structural assessment of underbridges, 1–451. NR/GN/CIV/025. London: Network Rail.
- Network Rail. 2013. BCMI DATABASE issue 4 user manual. London: Network Rail.
- Network Rail. 2019. NR/l3/CIV/006 Part 1D: Creating and maintaining structure hierarchy, 1–82. London: Network Rail.
- Ng, S., and F. Moses. 1996. "Prediction of bridge service life using time-dependent reliability analysis." In *Proc.*, 3rd Int. Conf. on Bridge Management, 26–33. London, UK: CRC Press.
- Olsson, A., G. Sandberg, and O. Dahlblom. 2003. "On Latin hypercube sampling for structural reliability analysis." *Struct. Saf.* 25 (1): 47–68. https://doi.org/10.1016/S0167-4730(02)00039-5.
- Paik, J. K., J. M. Lee, and M. J. Ko. 2003. "Ultimate compressive strength of plate elements with pit corrosion wastage." *Proc. Inst. Mech. Eng.*, *Part M: J. Eng. Marit. Environ.* 217 (4): 185–200. https://doi.org/10 .1177/147509020321700402.
- Paik, J. K., A. K. Thayamballi, Y. I. Park, and J. S. Hwang. 2004. "A time-dependent corrosion wastage model for seawater ballast tank structures of ships." *Corros. Sci.* 46 (2): 471–486. https://doi.org/10.1016/S0010 -938X(03)00145-8.
- Petrone, C., T. Rossetto, and K. Goda. 2017. "Fragility assessment of a RC structure under tsunami actions via nonlinear static and dynamic analyses." Eng. Struct. 136: 36–53. https://doi.org/10.1016/j.engstruct.2017.01.013.
- RAIB (Rail Accident Investigation Branch). 2010. Derailment of a freight train near Stewarton, Ayrshire 27 January 2009. Derby, UK: RAIB.
- Reddy, J. N. 2006. Theory and analysis of elastic plates and shells. Boca Raton, FL: CRC Press.
- Rizzo, F., G. Di Lorenzo, A. Formisano, and R. Landolfo. 2019. "Time-dependent corrosion wastage model for wrought iron structures." *J. Mater. Civ. Eng.* 31 (8): 1–15. https://doi.org/10.1061/(ASCE)MT.1943-5533.0002710.
- RSSB (Rail Safety and Standards Board). 2021. Route availability number for assessment of compatibility between rail vehicles and underline bridges, 1–35. GERT8006 Issue 3. London, UK: RAIB.
- Rummey, G. D., and L. B. Dowling. 2004. "Towards a uniform bridge management system for Australia and New Zealand." In *Proc.*,

- Austroads Bridge Conf., 5th, Hobart, Tasmania, Australia. Washington, DC: National Academy of Sciences.
- Saad-Eldeen, S., Y. Garbatov, and C. G. Soares. 2011. "Experimental assessment of the ultimate strength of a box girder subjected to severe corrosion." Mar. Struct. 24 (4): 338–357. https://doi.org/10.1016/j.marstruc.2011.05.002.
- Shinozuka, M., M. Q. Feng, J. Lee, and T. Naganuma. 2000. "Statistical analysis of fragility curves." *J. Eng. Mech.* 126 (12): 1224–1231. https://doi.org/10.1061/(ASCE)0733-9399(2000)126:12(1224).
- Shuvalov, A., L. Safina, and M. Kovalev. 2020. "Experimental research of service actions influence on elastomeric bearings elastic properties." *IOP Conf. Ser.: Mater. Sci. Eng.* 869 (5): 052018. https://doi.org/10 .1088/1757-899X/869/5/052018.
- Silva, J. E., Y. Garbatov, and C. Guedes Soares. 2014. "Reliability assessment of a steel plate subjected to distributed and localized corrosion wastage." Eng. Struct. 59: 13–20. https://doi.org/10.1016/j.engstruct.2013.10.018.
- SIMULIA. 2014. Abaqus 6.14 documentation. Providence, RI: SIMULIA. Sipple, J. D., and M. Sanayei. 2015. "Full-scale bridge finite-element model calibration using measured frequency-response functions." J. Bridge Eng. 20 (9): 1–11. https://doi.org/10.1061/(ASCE)BE.1943 -5592.0000705.
- Soares, C. G., and Y. Garbatov. 1999. "Reliability of maintained, corrosion protected plates subjected to non-linear corrosion and compressive loads." *Mar. Struct.* 12 (6): 425–445. https://doi.org/10.1016/S0951-8339(99)00028-3.
- SteelConstruction.info. 2024. "Design for half-through construction."

 Accessed May 9, 2024. https://www.steelconstruction.info/
 Design for half-through construction#Structural behaviour.
- Sultana, S., Y. Wang, A. J. Sobey, J. A. Wharton, and R. A. Shenoi. 2015. "Influence of corrosion on the ultimate compressive strength of steel plates and stiffened panels." *Thin-Walled Struct.* 96: 95–104. https://doi.org/10.1016/j.tws.2015.08.006.
- Tamakoshi, T., Y. Yoshida, Y. Sakai, and S. Fukunaga. 2006. "Analysis of damage occurring in steel plate girder bridges on national roads in

- Japan." In *Proc., 22th US Japan Bridge Engineering Workshop*. Washington, DC: Office of Infrastructure Research and Development, Federal Highway Administration.
- Vagnoli, M., R. Remenyte-Prescott, and J. Andrews. 2018. "Railway bridge structural health monitoring and fault detection: State-of-the-art methods and future challenges." Struct. Health Monit. 17 (4): 971–1007. https:// doi.org/10.1177/1475921717721137.
- Wang, K., and M.-j. Zhao. 2016. "Mathematical model of homogeneous corrosion of steel pipe pile foundation for offshore wind turbines and corrosive action." Adv. Mater. Sci. Eng. 2016: 1–8. https://doi.org/10 .1155/2016/9014317.
- Wang, R., R. Ajit Shenoi, and A. Sobey. 2018. "Ultimate strength assessment of plated steel structures with random pitting corrosion damage." J. Constr. Steel Res. 143: 331–342. https://doi.org/10.1016/j.jcsr.2018.01.014.
- Wikipedia. 2024. "British rail class 66." Accessed September 25, 2024. https://en.wikipedia.org/wiki/British_Rail_Class_66.
- Wilkie, D., and C. Galasso. 2020. "Site-specific ultimate limit state fragility of offshore wind turbines on monopile substructures." *Eng. Struct.* 204: 109903. https://doi.org/10.1016/j.engstruct.2019.109903.
- Yang, Y., Q. Wu, Z. He, Z. Jia, and X. Zhang. 2019. "Seismic collapse performance of jacket offshore platforms with time-variant zonal corrosion model." *Appl. Ocean Res.* 84: 268–278. https://doi.org/10.1016/j.apor.2018.11.015.
- Zabel, V., and M. Brehm. 2009. "System identification of high-speed railway bridges." In *Weimar optimization and stochastic days* 5.0, 1–18. Weimar, Germany: Dynardo GmbH.
- Zhang, Z., R. De Risi, and A. Sextos. 2023. "Multi-hazard fragility assessment of monopile offshore wind turbines under earthquake, wind and wave loads." *Earthquake Eng. Struct. Dyn.* 52 (9): 2658–2681. https://doi.org/10.1002/eqe.3888.
- Zhu, M.-L., L.-Q. Zhang, S.-Y. Huang, and C.-X. Song. 2021. "Analysis of factors affecting horizontal displacement of pier top of high-pile and high-pier bridge." E3S Web Conf. 261 (1): 03044. https://doi.org/10 .1051/e3sconf/202126103044.